DERIVING INHERENT OPTICAL PROPERTIES AND ASSOCIATED INVERSION - UNCERTAINTIES IN THE NAIVASHA LAKE

SEMHAR GHEBREHIWOT GHEZEHEGN
March, 2011

SUPERVISORS:
Dr. Ir. Mhd. (Suhyb) Salama
Dr. Ir. C. M. M. (Chris) Mannaerts

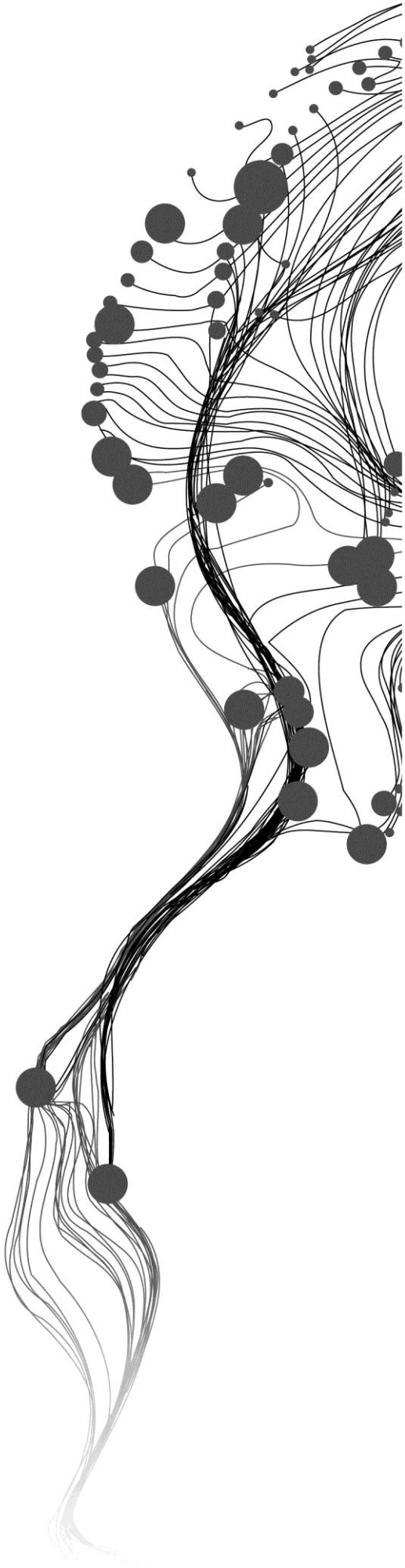

DERIVING INHERENT OPTICAL PROPERTIES AND ASSOCIATED INVERSION-UNCERTAINTIES IN THE NAIVASHA LAKE

SEMHAR GHEBREHIWOT GHEZEHEGN

Enschede, The Netherlands, March, 2011

Thesis submitted to the Faculty of Geo-Information Science and Earth Observation of the University of Twente in partial fulfilment of the requirements for the degree of Master of Science in Geo-information Science and Earth Observation.
Specialization: Water Resources and Environmental Management

SUPERVISORS:
Dr. Ir. Mhd. (Suhyb) Salama
Dr. Ir. C. M. M. (Chris) Mannaerts

THESIS ASSESSMENT BOARD:
Prof. Dr. Ing. W. (Woulter) Verhoef (Chair)
Dr. D.M. Harper, Leicester University, Department of Biology, UK (External Examiner)

ABSTRACT

Optical and Radiometric measurements were performed in Lake Naivasha in September 2010 for two weeks. The aim of this research is to determine the inherent optical property of the lake Naivasha and its associated inversion uncertainties using MERIS. The GSM semi-analytical inversion model is modified to include the absorption of non-algal particles and Phycocyanin. The concentration of suspended matter; absorption of chlorophyll-a, coloured dissolved organic matter (CDOM) and total absorption were determined from collected water samples in the laboratory. The modified model was validated using laboratory measured data set. The model was able to derive a linear relationship between measured and estimated IOPs with R^2 values above 0.7. The SPM concentration varies up to 20 mg/l per hour causing high variability in the derived NAP estimation. The model retrieves better high absorption of Chl_a (up to 3 m^{-1}) and indicates the co variance of phycocyanin absorption. Results obtained confirmed that Lake Naivasha is optically turbid, eutrophic lake with possible harmful algal bloom. The spatial analysis of the IOPs indicates that the flower farms located in the southwest and the hippo pool areas are the major contributors of high nutrient load as indicated by high CDOM and Chl_a absorption. In addition high back scattering of non-algal particles recorded near the Gilgil and Malewa river inlets. The environmental conditions such as wind direction play a major role in the spatial variation of the IOPs by re suspension of sediment at shallow depth and by transporting planktons. Inversion-uncertainties of the derived IOPs were also estimated using a standard nonlinear regression technique. The uncertainty of the inversion model decreased to a certain level and then starts increasing with water turbidity.

ACKNOWLEDGEMENTS

I would like to thank the Royal Netherlands Government who funded this study through the Netherland fellowship program. My deepest gratitude to ESA for providing the MERIS image as requested. It is a pleasure to thank those who made the fieldwork in Naivasha possible, Dr. David M. Harper for allowing us to use his laboratory, Mrs. Sarah Higgins, for providing the accommodation and permission to work in her property and I am grateful for Dr. Robert Becht for facilitating our work and transportation in Kenya.

I offer my sincerest gratitude to my supervisor, Dr. Suhyb Salama, who has supported me throughout my thesis with his patience and knowledge whilst allowing me the room to work in my own way. I also would like to thank Dr. Chris Mannaerts, my second supervisor, for his continuous support and guidance

My regards to my team who made the project successful and fun. I would like to thank to my friend, Elleni, who came all the way to Naivasha to see me and work with the team.

Last but not the least, I offer my regards and blessings to, all my family, friends and the one above all, the Almighty God, for answering my prayers and for giving me the strength to finish this thesis thank you so much Dear Lord.

TABLE OF CONTENTS

LIST OF FIGURES

LIST OF TABLES

NOTATIONS

Latin

$a(\lambda)$	Total absorption coefficient [m^{-1}]
a_{adg}	Absorption coefficient of CDOM+NAP [m^{-1}]
$a_{cdom}(\lambda)$	Absorption coefficient of CDOM [m^{-1}]
$a_{nap}(\lambda)$	Absorption coefficient of NAP [m^{-1}]
$a_{ph}(\lambda)$	Absorption coefficient of phytoplankton pigment [m^{-1}]
$a_w(\lambda)$	Absorption coefficient of water molecules [m^{-1}]
$\mathrm{a_p}(\lambda)$	Absorption coefficient of particulate [m^{-1}]
$A_{bs}(\lambda)$	Absorbance (optical density) value for a selected wavelength
A_f	Area of filter (m^2)
$b_b(\lambda)$	Total backscattering coefficient [m^{-1}]
$b_w(\lambda)$	Backscattering coefficient of water molecules [m^{-1}]
$bb_{spm}(\lambda)$	Backscattering coefficient of suspended particles [m^{-1}]
e_i	Residual at band i
E_o (λ)	Mean extraterrestrial irradiance
E_d (0^+)	Downwelling irradiance [$Wm^{-2}nm^{-1}$]
i	Iteration
L	Cross section of the cuvette (m)
L_w (0^+)	Water leaving radiance L_w [$Wm^{-2}sr^{-1}\ nm^{-1}$]
m	Number of unknown
n_w	Water index refraction
N	Number of bands
$Rs_w(\lambda)$	Water leaving Remote sensing reflectance [sr^{-1}]
R	The upper triangle matrix of QR of matrix decomposition
r^2	Correlation coefficient
t	Transmittance function
$T_v(\lambda)$	Diffuse transmittance from the target to the sensor
V_f	Volume of filter (m^3)

Abbreviations

IOPs	Inherent Optical Property
AOPs	Apparent Optical Property
NAP	Non Algal Particles
CDOM	Color Dissolved Organic Matter
MERIS	Moderate Resolution Imaging Spectra
SPM	Suspended Particulate Matter
LMA	Levenberg-Marquardt Algorithm
CZCS	Coastal Zone Color Scanner
NIR	Near Infra-Red
Chl_a	Chlorophyll a pigment
GF/F	Glass Fiber /Filter
TOA	Top Of Atmospheric
BOA	Bottom Of Atmospheric

Greek

η	The backscattering fraction
γ	The spectral slope of b_{spm}
τ	Optical thickness
ρ	Reflectance [%]
π	Pi
σ	Standard error
e	Error
χ^2	Chi-Square
θs	The Solar zenith angle [rad]
λ	Wavelength

1. INTRODUCTION

Lake Naivasha is located in the Kenyan part of the Great Rift Valley. It is a major tourist attraction due to its wildlife and beautiful landscape. However, it has now been degraded almost beyond recognition by eutrophication and pollution that is mainly due to the overuse of pesticides and fertilizers that wash into the lake. The two major tributaries of Lake Naivasha, Malewa and Gilgil Rivers, contribute 80% of the sediment load to the lake whereas the rest 20% is from the atmosphere (Kitaka et al., 2002; Rupasingha, 2002). Dr. David. M. Harper, who is Earth watch scientist at the University of Leicester, says,[1] "The Naivasha Lake is becoming an over-enriched muddy pool, which will shortly become unusable. Its inflowing rivers, formerly sparkling and permanent are now murky and unpredictable. As the lake becomes smaller and shallower, it will become warmer, fuelling the growth of microscopic algae. It is only a matter of time before the lake becomes toxic". In March 2010 after a heavy rain over 1000 fish were found dead. Indeed the Lake has become toxic. To monitor and quantify this water quality contamination by taking in situ measurement demands intense fieldwork, which is time consuming, and costly .Satellite remote sensing with its capability for large area and high temporal coverage was found to be very useful for monitoring water quality of lakes. Especially, ocean colour sensors have been used to obtain estimates of phytoplankton biomass, colour dissolved organic matter (CDOM) and water turbidity (Morel and Bélanger, 2006). Reliable monitoring of the suspended sediments or non-algal particles and harmful algal biomass in Lake Naivasha will require improved knowledge on the optical characteristics of water constituents, and better optical models relating the inherent optical properties (IOPs) of water constituents to the observed apparent optical properties (AOPs). Inherent optical properties (IOPs) are Properties that depend only on the water and other substances that are dissolved or suspended in it, as distinguished from apparent optical properties (AOPs) which are radiometric measurements that also depend not only on the substances in the water but also on the light field in which they are measured.
Empirical and semi-analytic algorithms have been developed to obtain estimates of IOP's from remotely sensed reflectance data. One of the advantages of semi analytical models over empirical ones is their capability to retrieve several parameters simultaneously and global application (Maritorena et al., 2002). One of the most used semi analytical model is the Garver-Siegel-Maritorena model abbreviated as GSM. This model is recently modified by Salama et al. (2009). The GSM model has been applied on open ocean (Maritorena et al., 2002) but has not been applied on eutrophic and optically turbid lakes. The aim of this research is to modify the GSM model and retrieve additional IOP such as the absorption of non-algal particulate of the highly degraded Lake Naivasha. Inaddtion the inversion uncertainty .of the model will be also evaluated.

1.1. Research Problem

Although non-algae particles (NAP) have significant absorption feature, their contribution to the total light absorption has been neglected by most studies and never been accounted for in the GSM model. Estimating the effect of NAP on the total absorption is very important to improve the accuracy of derived IOPs from semi-analytical models.

[1] Speech he gave on the fourth world water forum, in Mexico City on March 18th 2006.

1.2. Research Objectives

The main objective of this research is to modify the GSM model by accounting for the absorption of NAP. The following specific objectives are also defined:

- Radiometric measurement of water leaving radiances and laboratory analysis of water samples to retrieve absorption due to NAP.
- To include the absorption of NAP and its parameterization in the GSM model.
- Validate the modified model using in-situ measurements and MERIS images
- Estimate the inversion-uncertainties of derived IOP's.
- Map the derived IOPs of the lake Naivasha from MERIS images.

1.3. Research Questions

1) Does accounting for the absorption of NAP in the GSM model improve the accuracy of derived IOPs from MERIS's images?
2) Is there a way to de-convolve the absorption spectrum of NAP from that of CDOM?
3) What is the water quality status of the Lake Naivasha and how much NAP absorption contributes to the water clarity?

1.4. Research Hypothesis

Non-algal particulates (NAPs) play an important role in the total light absorption as one of the water constituents in the Lake Naivasha aquatic ecosystem.

2. STUDY AREA

2.1 Lake Naivasha

Lake Naivasha is located 100 km Northwest of Nairobi, Kenya. Administratively it is situated in the Naivasha Division of Nakuru District, Rift Valley Province. The geographic location of the study area lies between 00^0 40' to 00^0 53'S latitude and 36^0 15' to 36^0 30'E longitude. It is within the UTM zone 37. Altitude is around 1890 m. The water surface of the lake covers an area of about 130 km^2 with the average depth of 4m. The lake receives 90% of its discharge from Malewa, Gilgil Rivers. It is a fresh water lake surrounded by the alkaline lakes of Elmenteita, Nakuru, Magadi, and Bogoria. It is in a closed drainage basin and has no visible outlet. Climate ranges from humid to sub-humid in the highland and Semi-arid in the Rift Valley. The average monthly temperature ranges between 15.9 ^{0}C and 17.8 ^{0}C while minimum temperature is 6.8 – 8.0 ^{0}C and maximum temperature is between 24.6 –28.3 ^{0}C. The area has two rainy seasons short rainy season (mid-October to mid-December) and long rainy season (March to June) .Dry season occurs from December to February. There are generally calm conditions or slight winds in the morning over the lake. In the afternoon winds of 11-15 km/hr. are typical. Winds are strongest in August to October when they reach speeds of 21 km/hr. There are often violent storms over the lake leading to serious water movement. Natural Resources

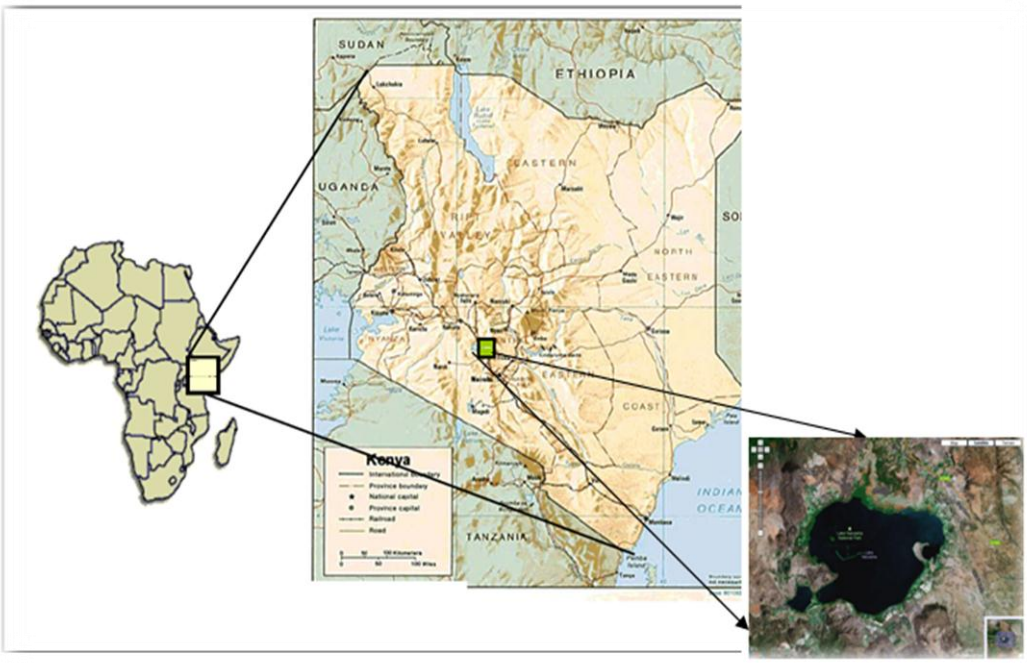

Figure 2-1: Location map of Lake Naivasha

2.2 Natural Resources

The birds of the lake are world famous hosting over 350 species. The diversity of wild life contributes to this area being an important tourist destination. The types of wildlife that are predominantly observed in

the study area are Giraffe, Zebra, Hippopotamus, Impala, and Waterbuck, Monkey, Buffalo and Warthog. These wildlife animals are mainly concentrated around the lake (riparian zone) and watering points. In addition, Lake Naivasha is an important site for commercial fisheries.

2.3 Geology

Volcanic rocks and quaternary lacustrine deposits cover the study area. The lake Naivasha basin, stretching over an area of 3292 km^2, lies in the East African Rift valley; major basin covers just over 2% of the continent and spread over seven countries, namely Djibouti, Eritrea, Ethiopia, Sudan, Uganda, Tanzania and including Kenya. Sediments cover much of the Rift Valley floor. These are Pleistocene in age; Quaternary era some 1.5 to 2.0 million years ago; and were laid down in lacustrine (lake) environments. The bulk of faults, scarps and fissures are linked with the Pleistocene movements. The volcanic rocks are a mixture of acid and basic larva's such as Tephrites, Rhyolites and Sodic Rhyolites (Tarras-Wahlberg et al., 2002).

2.4 Soils

Soils on the lacustrine plains around the lake have developed on sediments from volcanic ashes. Soils can vary from well to poorly drained, fine to sandy silts and clay loams of varying colour, but often pale. Generally, the soils are easy to work, but very powdery when dry. Soils in the catchment area are generally developed from volcanic activity, of moderate to low fertility, deep clayish loams, greyish brown to black in colour, often with drainage problems(Njenga et al., 2009).

2.5 Hydrology

Lake Naivasha with a total area of 13,255 hectares receives the discharge of the major rivers of Malewa, Gilgil and Karati. The flow from Karati is seasonal. Almost 80% of the inflow into the lake drained from Malewa with drainage area of about 1730 km^2 and Turasha sub catchments. Hydro-geologically, the lake Naivasha catchment is divided in to 11 sub basins namely Malewa, Gilgil, Karati, Turasha, Marmonet, Murukai, Kitiri, Wanjoni, Simba, Ngathi and Dundori. Other sources of water input in to the lake include rainfall that occurs directly over the lake through underground movements (groundwater flow) from the catchment. The outputs from the lake are direct evaporation from the lake surface, transpiration from the swamp and other aquatic vegetation, underground seepage and water extraction by human activities. Water balance of Lake Naivasha is has been studied by Becht & Harper (2002) and they estimated current annual abstraction rate of 60 x 10^6 $m^3 year^{-1}$, this is 6 times higher than that calculated as a ' safe' yield in the 1980's. Lake Naivasha catchment has no surface outlet. It has underground water inflows and outflows. The freshness of the water can only result of underground outflows; otherwise the lake water has been saline (Everard et al., 2002).

2.6 Economy and Environment

There has been tremendous agricultural and geothermal power development based on extraction of water from the lake with the cultivation of flowers and vegetables for the export market in Europe. Powerful extensive horticulture farms are located around the lake, producing 75% of Kenya's horticulture exports .There has been a rapid expansion of greenhouses mainly for flower cultivation around Lake Naivasha. Now over 100 large and small commercial farms are running irrigated floriculture. Due to this intense irrigation, the lake has become saline and eutrophic water. Over time, the quality of Lake Naivasha has been degrading becoming more salty and extensive reduction in size (Ballot et al., 2009).

2.7 Historical Data

Students from ITC have done extensive research on the Lake Naivasha and its surrounding since 1997. All thesis (over 50) combined contain a wealth of information on the climate, water and soil resources, the economy, the use and fate of pesticides and fertilizers, the land use and land tenure and the geology of the area. In addition for the last 20 years, Dr.D.M.Harper from Leicester university has lead the earth watch lakes of the rift valley research project to do a research on Lake Naivasha on its ecological cycle, phytoplankton community, contaminates and catchments. He compiled over 19 of his journals (Harper et al., 2003) regarding the lake and published it as a book called "Lake Naivasha, Kenya".

2.8 Water Degradation Problems in Lake Naivasha

The lake Naivasha has been shown a progressive change from fresh water lake to eutrophic lake due to high nutrient load in to the lake from the nearby agricultures and flower farms (Kitaka et al., 2002).The main sources of causes of eutrophication is the process of nutrient enrichment in water bodies, particularly from phosphorous and nitrogen (Wrigley and Horne, 1974). As nitrogen and phosphorous levels rise in water bodies, conditions become more conducive for blue-green algal blooms (Codd, 2000). As such, eutrophication is understood to prompt the frequency of blue-green algal blooms such as Phycocyanin (Codd, 2000). The present state of the Naivasha lake provide a good environment for cyanobacteria growth such as warm temperature, sun light, and nutrient concentrations (Wrigley and Horne, 1974). As this algal bloom die off, cell decay will start that leads to oxygen depletion that eventually kills Fish. Lake Naivasha has already experienced this event on March 2010 were over 1000 fishes where killed. Studies could not come up with definite reason on why this happen.

3. METHODOLOGICAL BACKGROUND

3.1 Inherent Optical Properties

As sunlight enters the water body, it interacts with the particulates and the dissolved materials within the water. When light interacts with particulates, the direction of propagation of the light can be changed through the scattering process, and part of the light may be absorbed by the particles and changed into other forms or wavelengths of energy. Similarly, dissolved materials may absorb light energy and convert it into other forms of energy. The absorption and scattering properties of a medium such as sea water are described by its inherent optical properties, or IOPs. IOPs are properties of the medium and do not depend on the ambient light field. That is, a volume of water has well defined absorption and scattering properties whether or not there is any light to be absorbed or scattered. This means that IOPs can be measured in the laboratory on a water sample, as well as in situ in the ocean. Hence, the absorption coefficient is the fundamental IOP that describes how a medium absorbs light. The volume scattering function similarly describes how the medium scatters light. Monitoring the IOP of water has been very helpful for understanding the most water quality degradation problems such as eutrophication and harmful algal blooms. Morel and Prieur (1977) introduced remote sensing method for water body classification based on their optical composition and complexity. Researchers generally divide the water types in to two categories based on their optical characteristic, case I and case II types.

Case I waters generally refer to open ocean waters which are optically simple. Phytoplankton and its byproducts dominate their spectral properties (Bricaud et al., 1998; Morel and Maritorena, 2001). In Case I water types the reflectance is a function of living algal cells, organic matter (NAP)from decay of algae and other living things, and dissolved organic matter (CDOM) from phytoplankton metabolism (Gordon et al., 1975). Case I waters are characterized by high photic depths (the depth at which irradiance is 1% of the value at the water surface) and higher concentration of algal pigments compared to other optically active constituents (Morel and Louis, 1977). Case II waters are optically complex bodies where phytoplankton, inorganic and organic particulate matter, and dissolved organic matter all significantly impact the water's spectral signature (Morel and Louis, 1977). Unlike Case I waters, suspended matter and dissolved organic matter present in the water column are not only the product of phytoplankton but can have terrigeneous sources and be spatially heterogeneous (Gallegos and Neale, 2002). Resuspension of bottom particles, terrigeneous colored dissolved organic matter, and anthropogenic particulate and dissolved substances can all impact the reflectance in Case II water body (Hommersom et al., 2009).

3.1.1 Colored Dissolved Organic Matter

Colored dissolved organic material (CDOM) is optically measurable component of dissolved organic matter in water. It is originated from decaying phytoplankton plants or carbon-based material. It consist of dissolved organic carbon in the form of humic acid (Stedmon et al., 2000). CDOM is also called with different names in some literatures such as aquatic humus, gilvin, yellow substances, humic substances, and gelbstoff (Binding et al., 2008; G. Dall'Olmo and A.A Gitelson, 2006).

CDOM absorbs blue to ultraviolent band and give water a yellowish to stained tea color. It is defined optically in absorption units m^{-1} though it is also reported as dissolved organic carbon (mg/L) (Kirk, 1976); Absorption by CDOM is inversely related to wavelength and is described by an exponential decay

curve (Binding et al., 2008). CDOM can reduce reflectance not only in shorter wavelength but in all visible wavelengths extending up to the lower NIR on high algae loaded water than the red absorption peaks (Dekker et al., 1991). Additionally, absorption by CDOM has been shown to increase uncertainty (error) in estimation of chlorophyll-a and suspended sediment in waters where CDOM is spatially heterogeneous (Garver and Siegel, 1997).

3.1.2. Total Suspended Matter

Total suspended matter (TSM) or seston refers to inorganic and organic material suspended in the water column. All particulate matter suspended in the water column that does not pass through a 0.45 μm filter. TSM is positively associated with turbidity and negatively associated with water clarity. The two main constituents of total suspended matter are non-algal particulate and plankton.

3.1.3. Non-Algal Particulate (NAP)

NAP also called tripton includes mineral particles from terrigeneous and anthropogenic origin; detritus matter primarily from the decomposition of phytoplankton, zooplankton cells, and plant debris. NAP can be optically diverse and may cause strong backscattering of incident radiation (Doxaran et al., 2002). When broken into its organic and inorganic components, the spectral characteristics of NAP are varied. Kirk (1976) reports organic NAP has absorption properties similar to CDOM. On the other hand, inorganic NAP causes strong scattering and low absorption in the water column (Babin et al., 2003; Magnuson et al., 2004). The backscattering due to mineral particles depends on junge size distribution, refractive index and apparent density of particles. These parameters are function of water content and vary according to organic or mineral origin of the NAP (Babin et al., 2003). During the high absorption of NAP in the visible band, Doxaran et al. (2007) conformed that the power law function fail to estimate the backscattering effect of particulate in the near IR band.In order to determine the affect of absorption of NAP on the shape of the backscattering spectrum, Doxaran et al. (2009) propose a model that determines the variation of backscattering spectra from the visible to the near IR . This model accounts the influence of particle size distribution and composition for both minerals and organic particle populations.

3.1.4. Phytoplankton

Phytoplankton is the main source of SPM light absorption. The most important pigment that affect water absorption is Chlorophyll-a. It has two strong absorption bands in the blue (443 nm) and red (675 nm) wavelength. The peak at the blue band is higher because of the accessory pigments which absorb light at the short wavelength(Gordon et al., 1975). The spectral variability can be caused due to cell size, pigment packaging affect, light penetration, nutrient abundance and pigment composition. Eutrophication and toxic algal bloom such as cyanobacteria are the main water quality contaminant caused by high amount of algal in water body (Wrigley and Horne, 1974). Both Chl_a and cyanobacteria exist together in algal bloom. Phycocyanin pigment (blue green algae) characterizes cyanobacteria and can be distinguishing easily by its maximum absorption at 620nm (Simis et al., 2005).

3.2. Models Developed to Estimate IOPs

Semi-analytic and empirical algorithms have been developed to obtain estimates of IOP's from remotely sensed reflectance data. Semi-analytic algorithms use approximations of radiative transfer and empirical relationships to provide invertible linkages between the AOPs and the IOPs (Gordon et al., 1988). Empirical algorithms, on the other hand, use statistical relationships to link observed reflectance ratios to measured IOP's of water constituents or their concentrations.

Development of semi-analytic algorithms has allowed the simultaneous retrieval of water constituents (IOPs) such as absorption of Chl_a, CDOM absorption and the backscattering of suspended particulates (Maritorena et al., 2002). On this research, the semi analytical method is adapted for the retrieval of IOP.

3.2.1. Semi Analytical Method

The remote sensing reflectance leaving the surface of water is related to the IOP's using the model(Gordon et al., 1988)

$$Rs_w(\lambda) = \frac{t}{n_w^2}\sum_{i=1}^{2} g_i \left(\frac{b_b(\lambda)}{b_b(\lambda)+a(\lambda)}\right)^i \quad (3\text{-}1)$$

Where, $Rs_w(\lambda)$is the remote sensing reflectance leaving the water surface at the wavelength (λ); g_i are constant taken from Maritorena et al.(2002); t and n_w are the sea-air transmission factor and water index of refraction, respectively .These values are taken from Gordon et al. (1988). The parameters b_b and a are the bulk backscattering and absorption coefficient of the water column, respectively.

The light field in the water column is assumed to be governed by four optically significant constituents, namely, chlorophyll-a (Chl_a), colored dissolved organic matter (CDOM), non-algal particulates (NAP) and suspended particulate matter (SPM). The absorption and backscattering coefficients are modeled as the sum of absorption and backscattering from water constituents:

$$a(\lambda) = a_w(\lambda) + a_{ph}(\lambda) + a_{cdom}(\lambda) + a_{nap}(\lambda) \quad (3\text{-}2)$$

$$b_b(\lambda) = bb_w(\lambda) + bb_{spm}(\lambda) \quad (3\text{-}3)$$

Where, the subscripts w denote water constituents; phytoplankton green pigment, ph; absorption effects of CDOM and NAP; and suspended particulate matter, SPM.

The scattering and absorption coefficients of water molecules, $b_w(\lambda)$, and $a_w(\lambda)$are assumed to be constant. Their values are obtained from (Morel, 1974; Pope and Fry, 1997), respectively. The total absorption of phytoplankton pigments $a_{ph}(\lambda)$ is approximated as

$$a_{ph}(\lambda) = a_0(\lambda) \times a_{ph}(440) + a_1(\lambda) \times a_{ph}(440) \times \ln(a_{ph}(440)) \quad (3\text{-}4)$$

Where $a_0(\lambda)$and $a_1(\lambda)$are statistically derived coefficients of Chl_a, their values are taken from (Lee et al., 1998). The absorption effects of NAP and CDOM are combined due to the similar spectral signature (Maritorena et al., 2002) and approximated using the model of (Bricaud et al., 1981):

$$a_{adg}(\lambda) = a_{adg}(440) \times \exp(-S_{adg} \times (\lambda - 440)) \quad (3\text{-}5)$$

Where, S represent the spectral exponent of combined effects of NAP and CDOM. The scattering coefficient of SPM, $b_{spm}(\lambda)$ is parameterized as a single type of particle with a spectral dependency exponent γ (Eisma and Kalf, 1987).

$$bb_{spm}(\lambda) = bb_{spm}(550) \times \left(\frac{550}{\lambda}\right)^{\gamma} \quad (3\text{-}6)$$

3.2.2. Inversion by spectral optimization

Garver & Siegel (1997) established a spectral optimization method for the inversion of ocean color spectra based on Eq.3.1 to determine three inherent optical properties (IOPs); the absorption coefficients for phytoplankton ,CDOM and NAP, and the backscattering coefficient due to particulates for the Sargasso sea. This model was modified by Maritorena et al.(2002) called GSM01. The modified model assumes the spectral shapes of the specific absorption coefficients for phytoplankton and dissolved and detritus materials and the specific backscattering coefficient for particulates are known or constant. This assumption were made to reduce the number of unknowns but remained the source of uncertainty to the inversion model (Maritorena et al., 2002). Salama et al.(2009) modified the inverse algorithm to include the spectral shape of dissolved and detritus materials (S) and the specific backscattering coefficient for particulates (γ). The numerical inversion is carried out using the constrained Levenberg–Marquardt algorithm (LMA), where the constraints are set such that they guarantee positive and physically meaningful values: the total numbers of parameters derived are five:

$$\mathrm{IOP} = \left[\mathrm{a_{ph}}(440), \mathrm{a_{dg}}\ (440), \mathrm{bb_{spm}}(550), \gamma, \mathrm{S}\ \right]$$

4. QUANTIFICATION OF IOPS AND THEIR UNCERTAINTIES

4.1. Field Measurements

Insitu sampling of inherent and apparent optical property were carried out from 17th September up to 3rd October. In addition, matchup measurements were taken every two days one hour before and after the MERIS satellite over pass. Total of 153 measurements were done from 56 sample points around the lake between 9 to 12 local time. The Lake has been covered three times during the project with the sampling interval has been between 150-300 m to match the MERIS pixel size. Measurements were only conducted during clear sky and calm condition of the lake. Water samples were kept cool using aluminium foil and analysed within 3 to 4 hrs after collection. The procedure for radiometric and lab analysis was adapted from IOCCG protocol (Mueller et al., 2003). Even though the Lake has been covered three times during the study, due to problem with data the first coverage (17-23 September 2010) is not included in this analysis

4.1.1 Inherent Optical Property Measurement

Water samples for laboratory analysis were obtained approximately 15cm below the water surface from each station and analysed for absorption of Chlorophyll-*a*, CDOM, total suspended and SPM concentration at the same day of sampling. The instrument used for measuring absorbance called UV/visible spectrophotometer. Reading for specific wavelength such as 400, 412, 440, 490, 555, 560, 620, 665, 680 and 750 nm has to be manually adjusted with this instrument. Blank sample was used for calibrating the spectrophotometer prior to reading the spectra of each wavelength. The concentration of SPM was determined using sensitive gravimetric method. The laboratory procedures were adapted from (Mueller et al., 2003).

Figure 4-1: Laboratory and radiometry field measurement in Naivasha Lake, Kenya

Absorption of Chl_a

Phytoplankton pigments (Chl_a) were initially extracted by filtering 150-300 ml of sample through Whatmann GF/F filters (0.45 μm) and grinding the filter paper with a glass rod after being submerged in 10 ml of 90% acetone. The solution was then filtered in 0.2 μm filter to extract remaining NAP. The test tubes were centrifuged at 2500 rpm (?) for 30 min, then transferred to 1cm glass cuvette, and read the absorbance in a spectrophotometer against acetone blank. The chlorophyll-*a* (a_{ph}) absorption coefficient was calculated using the following equation:

$$a_{ph}(\lambda) = 2.303 \times (A_{bs}(\lambda) - A_{bs}(750)) \times \frac{A_f}{V_f} \quad (4\text{-}1)$$

Where A_{bs}, A_f and V_f denote the absorbance (optical density) value for a selected wavelength, area of filter and volume of filter respectively. Absorbance at 750nm is used to correct for scattering affect.

CDOM absorption (a_{cdom})

CDOM is simply measured by filtering the sample by 0.2μm Whatmann GF/F filters. Dilute water has been used as a blank. The measured spectra were changed to absorption (a_{CDOM}) using the following equation: Absorbance at 750nm is used to correct for scattering affect within the cuvette.

$$a_{cdom}(\lambda) = 2.303 \times \left(\frac{A_{bs}(\lambda) - A_{bs}(750)}{L}\right) \quad (4\text{-}2)$$

L denotes the cross section of the cuvette, which is 0.01 m. The S slope coefficient in nm^{-1} is derived by applying nonlinear exponential fits to the absorption coefficients and wavelength as seen on eqn.3.

$$a_{cdom}(\lambda) = a_{cdom}(\lambda_0)e^{-s(\lambda-\lambda_0)} \quad (4\text{-}3)$$

Total absorption (a)

After shaking the sample bottle for any remaining settled sediment, the solution was poured in the cuvette and directly measured in the spectrophotometer. Absorbance at 750nm is used to correct for scattering affect within the cuvette.

$$a_{total}(\lambda) = 2.303 \times \left(\frac{A_{bs}(\lambda) - A_{bs}(750)}{L}\right) \quad (4\text{-}4)$$

Nap absorption (a_{nap})

The absorption value for NAP was determined by subtracting the absorption of chlorophyll-a and CDOM absorption from the total.

$$a_{nap}(\lambda) = a(\lambda) - (a_{ph}(\lambda) + a_{cdom}(\lambda)) \quad (4\text{-}5)$$

The S slope coefficient is derived by applying nonlinear exponential fits to the absorption coefficients and wavelength.

$$a_{nap}(\lambda) = a_{nap}(\lambda_0)e^{-s(\lambda-\lambda_0)} \quad (4\text{-}6)$$

4.1.2 Apparent optical property measurement

The instrument used this measurement is Trios RAMSES with sensors such as radiance (7° field of view) and ACC-VIS irradiance sensor (380 – 950 nm). The remote sensing reflectance is calculated using the ratio of water leaving radiance [Lw ($Wm^{-2}sr^{-1}$ nm^{-1})] to downwelling irradiance just above the water surface[E_d (0^+) ($Wm^{-2}nm^{-1}$)].

$$R_{rs} = L_w (0^+) / E_d (0^+), (sr^{-1}) \quad (4\text{-}7)$$

The measurements have been performed 5 times per site for data quality. During the surface measurements of the water, leaving radiance at zenith angle is ~30° in order to avoid sun glint. During processing 95%, confidence interval has been taking for data validation. Hence, the wind speed in the lake is less than 5m/s; it is assumed the surface reflectance to very low. Measurements have been done in a clear sky, toward the sun to avoid shadow (Figure 4-1). Additional optical measurements have been done for match up sampling one hour before and after MERIS over pass. The measurement has been done in a loop style in which the starting and finishing point is the Crescent Lake.

4.2. MERIS Matchup Dataset

Medium spectra Full resolution (MERIS) levels 1b were used for deriving IOPs. MERIS has high spectral and radiometric resolution with high sensitivity of (1650) signal to noise ratio (Appendice-2). ESA provided the MERIS image as requested but due to high cloud coverage in the study area only 4 cloud free images (17, 20, 23 and 26 September 2010) were retrieved for match-up dates. The match-up samples were taken 1hr before and after the MERIS satellite overpass time.

Table 4-1 Downloaded MERIS images for Match-up

Date	MERIS FR data	Solar zenith angle
17/09/10	MER_FR__1PNUPA20100917_071754_000000982093_00049_44692_0517	31.2
20/09/10	MER_FR__1PNUPA20100920_072334_000000982093_00092_44735_0518	30.8
23/09/10	MER_FR__1PNUPA20100923_072915_000000982093_00135_44778_0521	31.0
26/09/10	MER_FR__1PNUPA20100926_073453_000000982093_00178_44821_0520	25.7

4.3. Algorithm development

The modified GSM will incorporate additional absorption due to NAP and phycocyanin. Based on the forward model (Eq. 3.1), the two main IOPs ($a(\lambda)$ & $b_b(\lambda)$) are partitioned to the following components:

$$a(\lambda) = a_w(\lambda) + a_{ph}(\lambda) + a_{cdom}(\lambda) + a_{nap}(\lambda) + a_{pc}(\lambda) \quad (4\text{-}8)$$

The $a_w(\lambda)$ is constant (Pope and Fry, 1997); $a_{ph}(\lambda)$, $a_{cdom}(\lambda)$, $a_{nap}(\lambda)$ and $a_{pc}(\lambda)$ are absorption due to phytoplankton, CDOM, NAP and Phycocyanin respectively. The total backscattering is characterized by the summation of back scatting of water molecules which are constants taken from Pope and Fry (1997) and the backscattering of particles/SPM Eq (3-3).

Parameterization of IOPs are adapted from Eq (3.4) - Eq (3.6). In order to isolate the absorption of phycocyanin from other phytoplankton species band 620 nm where only the absorption phycocyanin is

dominant (Simis et al., 2005). During the derivation of parameters such as $a_{ph}(\lambda)$,$a_{cdom}(\lambda)$, $a_{nap}(\lambda)$ the wavelength 620 nm where excluded.

$$a_{pc}(620) = b_b(620)\left[\frac{f}{R_{rs}(620)} - 1\right] - (a_w(620) + a_{ph}(620) + a_{cdom}(620) + a_{nap}(620)) \quad (4\text{-}9)$$

Where, $f = \frac{t}{n_w^2}$

Insitu data for phycocyanin has not been done .hence the retrieval accuracy of the model is tested by assuming the co-existence of Chl_a and phycocyanin during algal bloom or in eutrophic water (Simis et al., 2005)

The absorption of NAP will reduce the backscattering efficiency of SPM at the blue wavelengths by Δb_p. Doxaran et al., (2009) proposed a model that estimates the values of Δb_p. The GSM01 model assumed that the $\Delta b_p \sim = 0$, it is clear that such assumption overestimates the particulate backscattering and results in significant errors (Figure 4-2). The reduction of backscattering coefficient was computed as (Doxaran et al, (2009):

$$\Delta b_p = a_p(1 - \tanh(0.5 \times \gamma^2)) \quad (4\text{-}10)$$

$$bb_p(\lambda) = b_b(\lambda_{ref}) \times \left(\frac{\lambda}{\lambda_{ref}}\right)^{-\gamma} - [1 - \tanh(0.5 \times \gamma^2)] \times a_p(\lambda) \quad (4\text{-}11)$$

Where, λ_{ref} stands for the reference wavelength and γ is the spectral slope of $b_p(\lambda)$ both in spectral domain, where particulate absorption is almost negligible, i.e., the near IR.

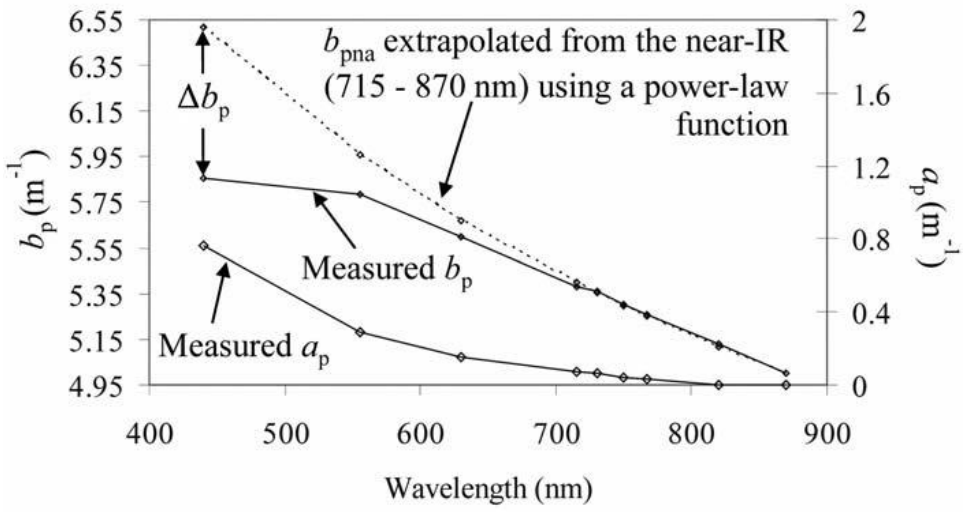

Figure 4-2: The error propagated due to over estimation of bbnap adapted from Doxaran et al. (2009)

The modified GSM model is adapted to derive eight parameters in visible bands covering the wavelength From 400 nm to 850 nm. The above equation were written as a code in interactive data language (IDL) format and apply to the ground measured Rrs dataset and MERIS images.

4.3.1 Model Inversion

The unknown IOPs are derived by fitting the modelled Rrs to the measured Rrs. a method of least-square minimization is adapted to retrieve the derived IOPs (Salama et al., 2009). Least-square minimization is a special case of chi-square minimization (maximum likelihood estimation) of the fitted parameters (Appendices 3).

$$\emptyset = \sum_{i=1}^{N} \left[Rrs_{w,m}^{(\lambda_i)} - Rrs_{w,d}^{(\lambda_i)}(IOP) \right]^2 \quad (4\text{-}12)$$

The minimum difference will be the best-fit .The constraints are set in such a way that they guarantee positive values of retrieved IOPs. Initial values where adapted from Lee et al. (2002) (Appendices 3). In order to reduce the degradation of the model in MERIS unknowns such as spectral slope of cdom and nap and the back scattering coefficient where remained constant. The total numbers of out puts derived from the MERIS images are:

$$IOP = \left[a_{ph}(440), a_{cdom}(440), a_{nap}(440), a_{pc}(620), b_{spm}(550) \right]$$

4.4. Error analysis (uncertainty)

The deviation of model prediction from measured spectra (i.e. error) can be assigned to the sensor's noise, imperfect atmospheric correction and model inversion (Salama and Stein, 2009). In this paper, only the inversion uncertainty due to model inversion is a discussed. It is difficult to decompose the error due to model inversion to individual IOP. Hence, the error between derived and measured is used as an inversion uncertainty or error. If the error between derived and measured IOP is assumed normally distributed, the variance of the estimate can be estimated as (Smyth, 2006):

$$\sigma = \frac{1}{N-m} \sum_{i=1}^{N} e_i^2 \quad (4\text{-}13)$$

Where (N-m) is the degree of freedom , number of bands (N) minus the number of unknown (m). The term e_i is the error between measured and derived IOP (Y_p) at a band (i).The confidence interval, $ci(Y_p)$, for model's best retrieved IOP can be then approximated as (M.Bates and G.Watts, 1988; Maritorena and Siegel, 2005):

$$ci(Y_p) = \pm\sigma \, \| QR(V)^{-1} \|_p^{\frac{1}{2}} \, t(N-m; \alpha/2) \quad (4\text{-}14)$$

Where $t(N-m; \alpha/2)$ is the upper quantile for student's t distribution with N-m (degree of freedom).The Matrix $\| QR(V)^{-1} \|_p^{\frac{1}{2}}$ the length of the pth row of the inverted and QR decomposed matrix of partial derivatives V, of the model (Eq 2-1) with respect to each unknown.

In addition, mean, standard deviation, correlation coefficient, root mean square errors were computed between derived and measured IOPs. The RMSE is calculated based on:

$$RMSE = \sqrt{\frac{\sum (IOP_{derived} - IOP_{measured})^2}{n}} \quad (4\text{-}15)$$

The role of NAP from the total absorption was calculated as follows:

$$a_{nap}(\%) = 100 \times \left(\frac{a_{nap}(\lambda)}{a(\lambda)} \right) \quad (4\text{-}16)$$

5. RESULTS

5.1 Insitu Inherent Optical Properties (IOPs)

5.1.1 Chlorophyll-a absorption

The average chlorophyll-a absorption at 440nm measured is 2.380 ± 0.433m^{-1} with maximum up to 3.283± 0.433m^{-1} around the Crescent Lake and the northwest part of the lake and the minimum absorption 1.142 ± 0.433 m^{-1} was measured in middle part of the main lake. The higher absorption value in the north west part of the lake is probably due to a very shallow nature of the lake (<1m) which is populated by submerged and emergent plant as explained by Harper et al.(1995). Most of the plant species encountered during the fieldwork including algal bloom are shown in Figure 5-1. The overall Chl_a absorption value of the lake is similar with eutrophic lake such as Lake Taihu, which has a range of absorption between 0.24-3.63m^{-1}(Sun et al., 2009).

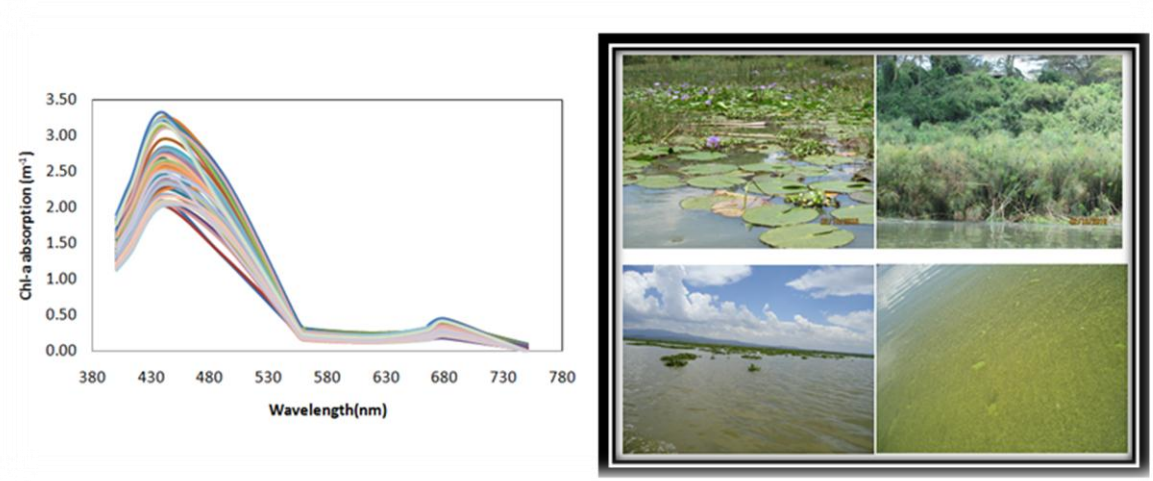

Figure 5-1: Absorption spectra of Chl_a (left); and the type of plants and algal colony in lake Naivasha (right)

5.1.2 CDOM absorption

The average CDOM absorption coefficient recorded at 440 nm was 2.468 ±0.604 m^{-1} with maximum value 3.455±0.604 m^{-1}, which is recorded around the northwest part of the lake and minimum absorption 0.921±0.604 m^{-1} in the eastern part of the lake. The values of the slope (S_{cdom}) coefficient range between 0.01-0.026±0.003 nm (figure 5-2).

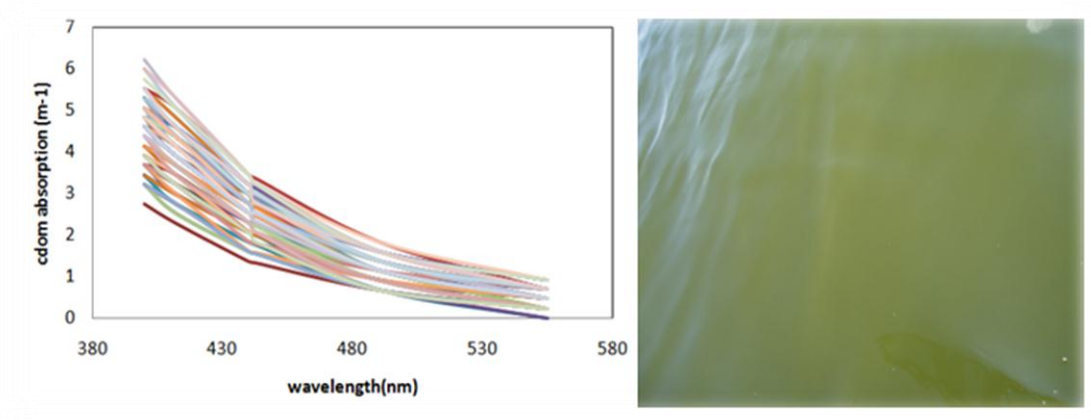

Figure 5-2: Insitu measured absorption of CDOM (left) and greenish brown colour of the Lake (right)

5.1.3 Total absorption

The average value was 10.217±3.059 m^{-1} with maximum value recorded 19.236±3.059 m^{-1} in the Malewa River in flows and the minimum value recorded is 3.691±3.059 m^{-1} in the Crescent Lake. The total absorption value highly varies depending on the absorption value of NAP and Chl_a, which are variable spatially and temporally. Whereas the absorptions of CDOM remains relatively constant. As seen on Figure (5-3), the total absorption is dominated by NAP. The average contribution of NAP to the total absorption is ~54%.

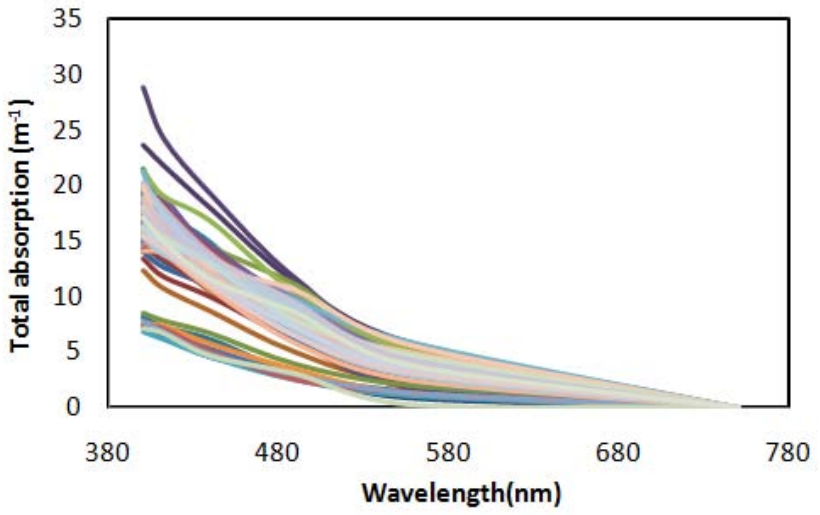

Figure 5-3: Insitu total absorption

5.1.4 NAP absorption

The average NAP absorption value was 5.55 ± 2.94 m^{-1} with maximum NAP value 14.93 ± 2.94 m^{-1} that located in the Malewa River inlets and the minimum 0.01 m^{-1} in the Crescent Lake. The NAP absorption value is 2-3 times higher in amount to previous studies made in eutrophic lakes (Babin et al., 2003; Sun et al., 2009) but similar with turbid lakes (G. Dall'Olmo and A.A Gitelson, 2006). The value of the slope (S_{nap}) coefficients range between 0.001- 0.006 ± 0.0007 nm^{-1} with average 0.004± 0.0007 nm^{-1} .As seen on Figure 5-4, the NAP shows different pattern those with absorption below 5m^{-1} ,these are samples taken from the Crescent Lake .

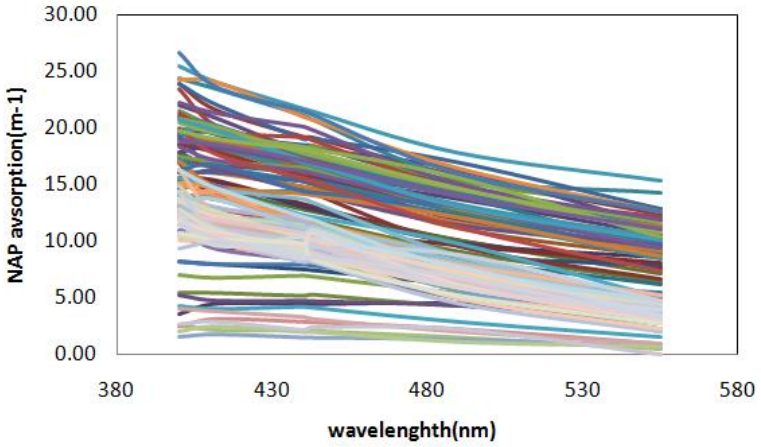

Figure 5 4 Insitu measured absorption of NAP

5.1.5 SPM concentration

SPM is one of the most variable parameter in the lake. The southeast wind (dominant wind direction during the study period) plays a major role by re suspending the bottom sediments. Because of this, within one hour difference the SPM concentration of rise up to 20 mg/l. Large variation has been noticed on the northern shallow part of the lake. The average value was 29.92 ± 12.27 mg/l with maximum 58.33±12.27 mg/l measured at the Malewa River in flow and minimum 1.00±12.27 mg/l measured at the Crescent Lake.

Table 5-1: Statistical summary of the analysis of Insitu IOP parameters

IOPs	Max	Min	Average	Stdev
Chl_a	3.283	1.142	2.380	0.433
CDOM	3.455	0.921	2.468	0.605
Total_abs	19.236	3.691	10.217	3.059
NAP	14.935	0.000	5.551	2.939
SPM	58.333	1.000	29.923	12.270
S_CDOM	0.026	0.010	0.0135	0.003
S_NAP	0.007	0.001	0.004	0.001

5.2 Insitu Remote Sensing Reflectance (Rrs)

Insitu measurements of remote sensing reflectance were strongly dominated by absorption from NAP (composed of detritus and minerals), phytoplankton pigments, CDOM, and scattering from suspended inorganic matter. As seen on figure 5.5, the low signal from 400 to 470 nm appears to be caused by strong absorption from high concentrations of detritus and mineral particles. NAP, which absorbs most strongly in the blue has been found to be the main absorbing component (up to 79%) in other similar eutrophic and turbid lakes (Zhang et al., 2007).There was very little upwelling light in the blue (500 nm), strong absorption at 620 and 680 nm characteristic of Phycocyanin and Chl_a pigments, and strong reflectance peak at 560 and 710 nm. The sharp peak near 710 nm was correlated with Chl_a and suspended solids (Doxaran et al., 2007). It appears that scattering by particulate matter is the dominant in the lake. The relative invariance of the shapes of the spectra indicates that the IOPs were relatively constant for the

duration of sampling but the differing magnitudes of the spectra are likely to be caused by variable concentrations of phytoplankton and TSS, especially for the northern part of Lake and the Gilgil in late.

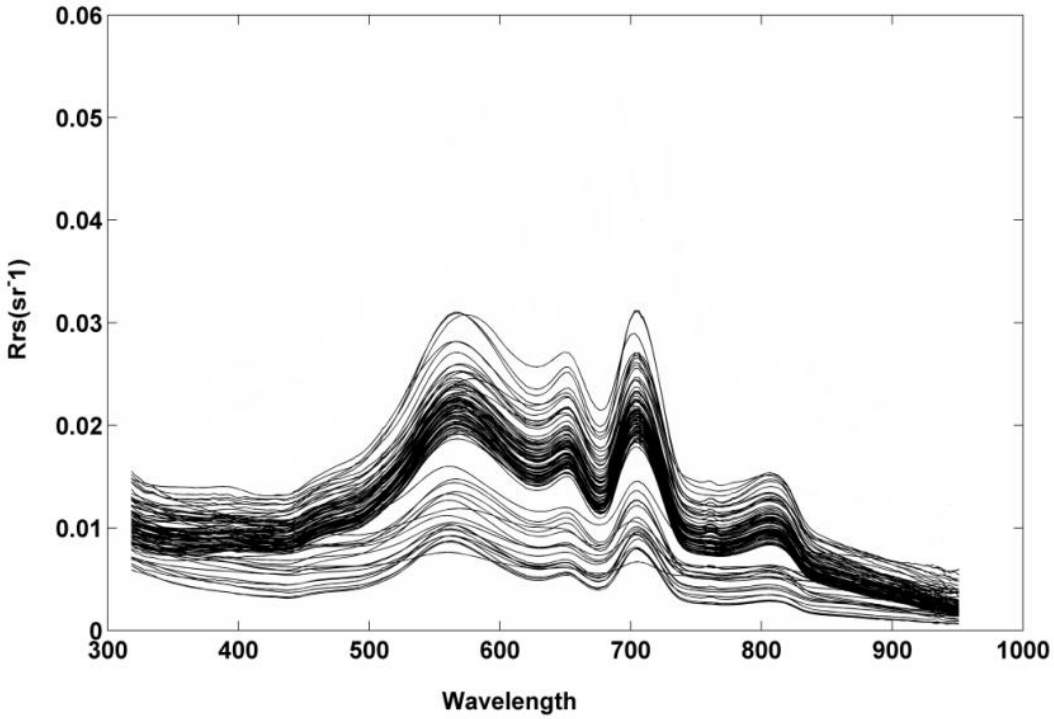

Figure 5-5 Ground measured remote sensing reflectance

5.2.1 Deriving IOPs using insitu Rrs

The derived IOPs using the TRIOS RAMESE ground measurement gives a good a linear relationship between measured and estimated IOPs with R^2 values above 0.7 and RMSE <1.8 (Figure 5.6). Its' Chl-a absorption varied within the range 3.4- 4 m^{-1},Phycocyanin absorption 1.3-3 m^{-1}, absorption of the CDOM 0.8-1.8 m^{-1}, absorption of NAP 2–2.25 m^{-1} and total absorption ranges between 8.2-10.2 m^{-1} backscattering coefficient 1.2–1.8 m^{-1} . The spectral slopes for CDOM and NAP ranges between 0.001 - 0.03 and 0.005-0.023 nm^{-1} respectively. All IOPs were underestimated by the model except for Chl_a absorption (Figure 5.6-a). From the plot, it is easily noticed a cluster of points (Chl_a and b_{spm}) that characterize the Crescent Lake, which has higher Chl_a, and lower NAP content as compared to the main lake.

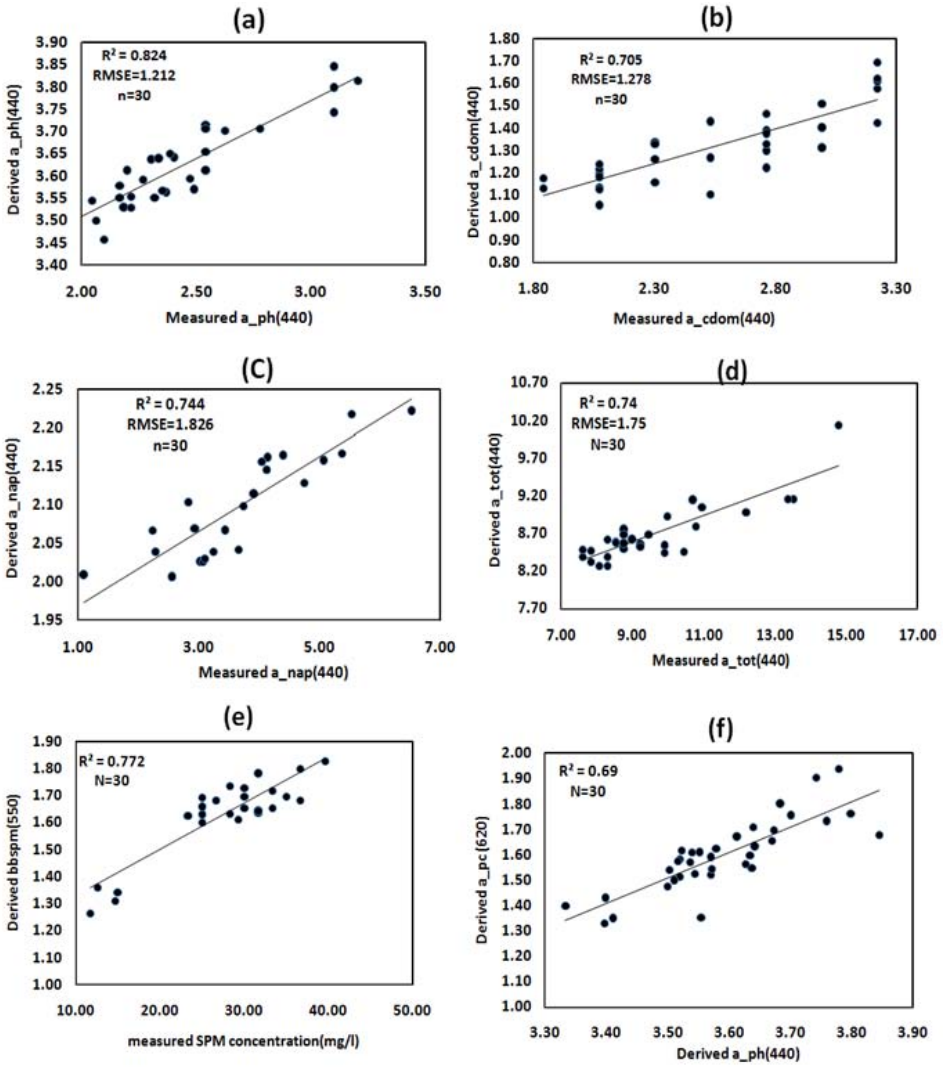

Figure 5-6 Derived IOPs as compared with the measured IOPs

5.3 Atmospheric Correction

One of the most difficult task in monitoring the inland water quality or highly turbid water bodies is the atmospheric correction. In open ocean, atmospheric correction methods are generally based on the dark pixel method or assuming that radiance is nearly zero at the NIR (Siegel et al., 2000). But in inland water bodies such as Naivasha Lake the observed radiance in the NIR is affected by the backscattering of high concentration of suspended particles (Babin et al., 2003). Hence, applying the method of dark pixel will cause negative value in the blue band.More recently developed atmospheric correction schemes such as the Self-Contained Atmospheric Parameters Estimation for MERIS data (SCAPE-M) which calculate the reflectance of close-to-land water pixels through spatial extension of atmospheric parameters derived over neighboring land pixels (Guanter et al., 2010) where not considered on this paper because the plug in has not been released yet .The SCAPE-M plug-in provides good considerable improvement of atmospheric over turbid waters. This research is using curve fitting (least square minimization) between the matchup MERIS and ground measured Rrs to determine the path radiance and the diffuse transmittance.

The most dominate atmospheric effect on remote sensing is path radiance which is the scattering of radiation from the sun's beam into the direction of the satellite by air molecules or by suspended particles (Deschamps et al., 1983). In addition, Diffuse transmittance from the ground to the sun play also a role in the scattering of light .To focus more to path radiance the following assumption where made: Absorption and emission of radiation by gas, overall effect on object illumination scattering of reflected radiation out of the sensor view where neglected. The top of atmosphere radiance is given by:

$$L_{TOA}=L_{path}+L_{BOA}e^{-}\tau/\cos\theta \quad (5\text{-}1)$$

L_{TOA} is the radiance at the top of atmospheric, which can be retrieved from MERIS image directly. L_{path} and L_{BOA} is the path radiance and bottom of atmospheric (surface) radiance respectively and $e^{-}\tau/cos\theta$ is the diffuse transmittance as a function of optical thickness τ and viewing angleθ. The path radiance and diffuse transmittance value where derived using curve fitting procedure against the insitu measured remote sensing reflectance in which the minimum root mean square error accepted (Appendix 1). To calculate the reflectance at the bottom of atmospheric (BOA) the following formula is adapted (Moran et al., 1992):

$$\rho_{BOA}=\frac{\pi(L_{TOA}-L_{path})}{E_{o(\lambda)}\cos\theta_s T_v} \quad (5\text{-}2)$$

Where $E_o(\lambda)$ is Extra-terrestrial solar irradiance corrected for earth-sun distance and θs represents the solar zenith angle. The solar spectral irradiance ($E_0(\lambda)$) can be estimated as (Deschamps et al., 1983)

$$E_0(\lambda)=H_0(\lambda)\left(1+e\cos\left(\frac{2\pi(D-3)}{365}\right)\right)^2 \quad (5\text{-}3)$$

Where $H_0(\lambda)$ is the mean extraterrestrial irradiance obtained from Neckel and Labs (1981), e=0.0167 is orbital eccentricity and D is the Julian day. The water leaving remote sensing reflectance is calculated by dividing the BOA reflectance by pi. For validation images from of 20, 23 and 26 September 2010 were used.

$$Rrs(sr^{-1})=\frac{\rho_{BOA}}{\pi} \quad (5\text{-}4)$$

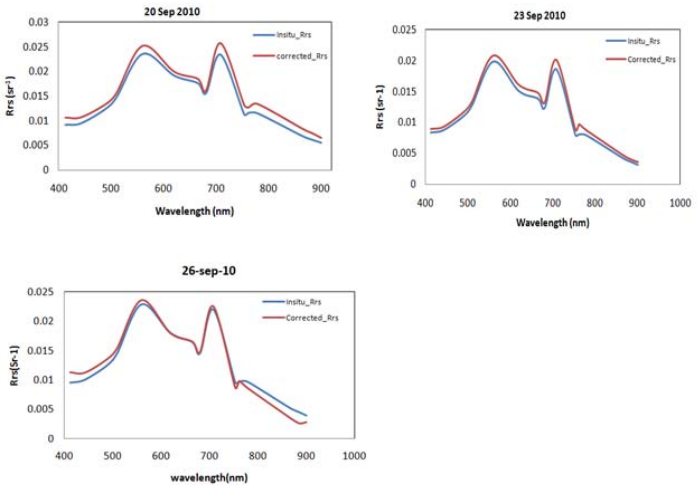

Figure 5-7 Validation of atmospherically corrected image with insitu measured Rrs

In order to avoid the adjacency affect, the points near to the land surface were removed from validation. As seen from Figure 5-7, the atmospheric correction has been shown good result during validation with Ground measured Rrs.

5.3.1 Deriving IOP's using Rrs from MERIS image

The derived IOPs show good correlation with R^2 values > 0.75. The RMSE of total absorption and NAP increased more than three times higher than the Nap derived from the ground Rrs measurement. (Figure 5.8- c and d). This could be due to the spectral resolution of MERIS and hence the fewer degree of freedom of the inversion model.

Its' Chl_a absorption varied within the range 3.2- 3.5 m^{-1},Phycocyanin absorption 1.2-1.5 m^{-1}, absorption of the CDOM 1-1.5 m^{-1}, absorption of NAP 2.09–2.18 m^{-1} , total absorption ranges between 7.75-8.12 m^{-1} and backscattering coefficient 1.7–2.1 m^{-1} . The model underestimated all IOPs except Chl_a absorption.

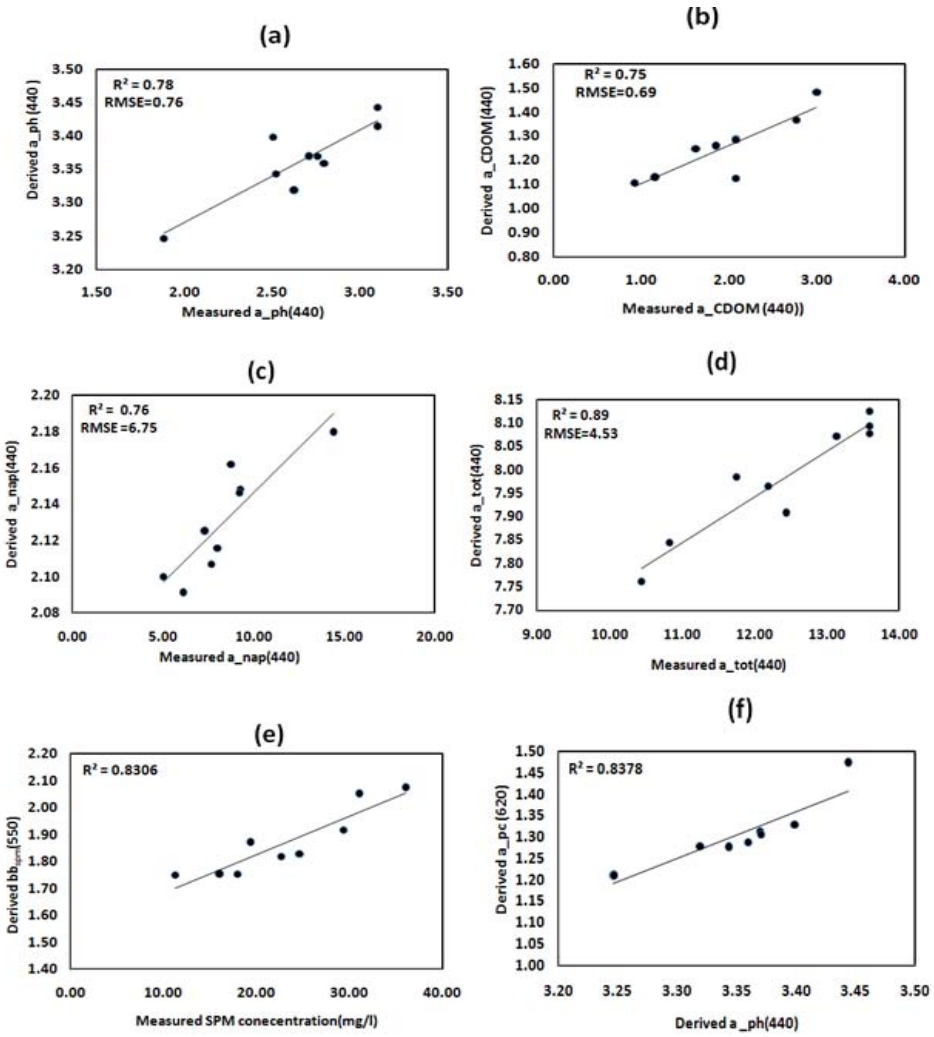

Figure 5-8 Validation of IOP's derived from MERIS using lab measured IOPs

5.4 Uncertainties

5.5.1 Uncertainties due to insitu measurements

Windy conditions (>5m/s) cause high wave action that mixes buoyant phytoplankton and sediments composed mainly of organic detritus from the lake floor to the surface (Fitch and Moore, 2007). The Insitu sample collected shows a highly variable absorption over the lake for a different day events.
The standard error (Table 5-2) of the mean for in situ samples ranged from 6.09 to 33.36%. In contrast the standard error of the mean for the derived IOP's estimates was smaller, ranging from 1.005 to 4.13%. Thus the large uncertainties involved with estimating the mean absorption for the lake with only a few in situ measurements is decreased through using remote sensing. The observed error, the difference between mean remotely sensed and in situ measurements, is as large as 30%. Therefore, assuming that the true mean for the lake is the remotely sensed estimate, approximating the mean using in situ measurements alone in this case may be up to 30% in error, although this error is reduced by increasing the number of sample points and repeated sampling of the lake (3 times). This kind of uncertainty has been noticed on the validation of the MERIS derived and insitu measured IOPs. Inaddtion the sampling depth of ~15cm could also be a source of uncertainty for it characterizes stratified zone of the water column.

Table 5-2 : Average standard error between IOPs

	Chl_a	CDOM	NAP	Total-abs
MERIS-IOP	1.9205	4.0880	1.0047	4.1390
Insitu-IOP	6.0707	8.2889	20.9066	33.3600

5.5.2 Uncertainties due to model inversion

The overall absorption show unique pattern in both positive and negative correlation as indicated by red lines. The error decreased to a certain level and then starts increasing with water turbidity (Figure 5-11). Melin (2010) also come up with similar graphs while mapping global Chl_a concentration . Even tough the consideration of NAP absorption for the GSM model reduce the error due to overestimation of backscattering coefficient ,still over 100% uncertainties have been noticed in the majority of IOPs. This is caused by a large inversion error in case II water with high value of scattering and absorption.

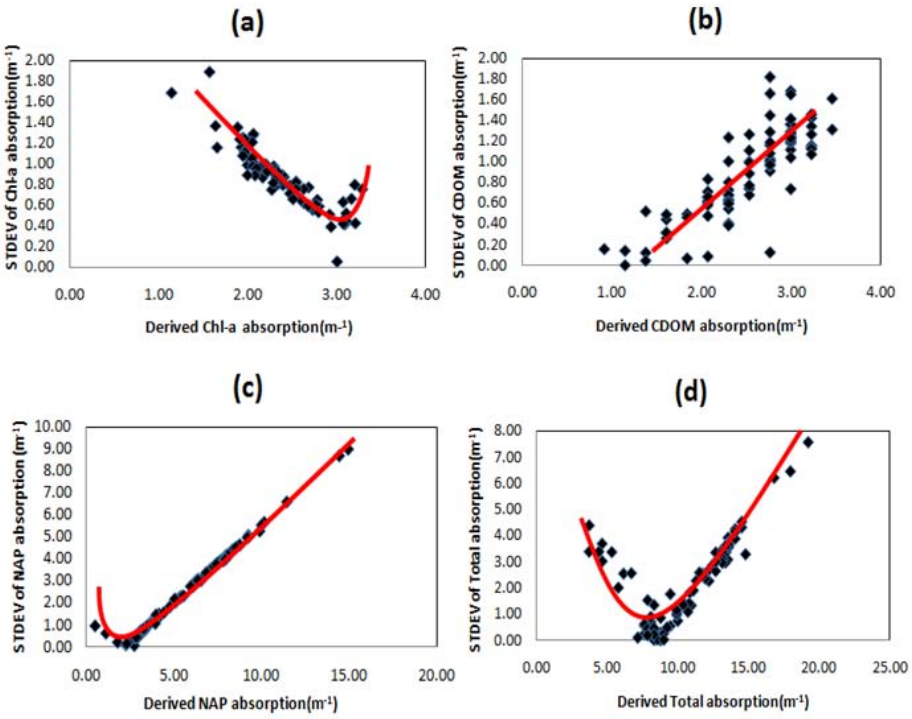

Figure 5-9 : Uncertainty analysis between Derived IOPs and the standard deviation of measured and derived IOPs

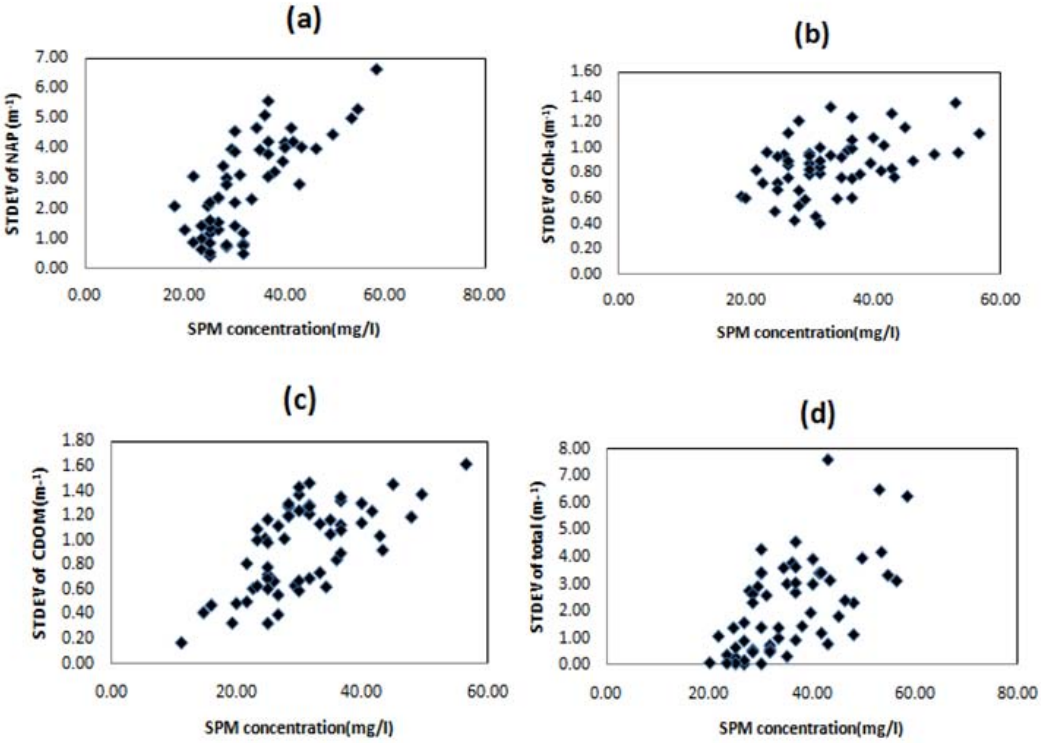

Figure 5-10: Uncertainty analysis between SPM/turbidity and the standard deviation of measured and derived IOPs

5.5 Spatial Distribution of IOPs

In a shallow lake such as Lake Naivasha, the waves create turbidity by re-suspension of sediment at depth reducing primary production by minimizing the effects of light penetration. Wind speeds greater than or equal to 2–3 ms^{-1} are sufficient for mixing the upper 0.5 m of the water column, and speeds of greater than approximately 6 ms^{-1} are sufficient for mixing to up to 1.9 m depth of lakes (Matthews et al., 2010).
Maps to see the distribution of IOPs were made for each water quality parameter using the modified GSM algorithm on MERIS images taken on the 20th and 26th of September 2010. The maps were plotted as false-colour plots using ENVI_IDL software; the colour bar indicates the unique value of each pixel. The image for the 20th where taken while the lake was in the clam condition with no wave. Whereas the image at the 26th is taken while the lake was disturbed by the windy condition. This helps the research to understand the impact of environmental conditions to the spatial variability of the IOPs.
To visualize the spatial variability of the IOPs, Lake Naivasha partitioned into five different categories based on the location, soil types, and plant life's and animal inhabitants. The five major parts of are; The Crescent Lake, the inlets for Gilgil and Malewa ,flower farms and wet lands located in the northwest part of the lake, the Hippo pool in which over 1000 hippos located (local source) and the south eastern flower farms. The following analysis was based on the insitu data collected from September 23 up to October 03 2010. In this period the lake has been covered twice.

5.5.1 The Crescent Lake

The Crescent Lake shows relatively constant absorption of Chl_a, CDOM, NAP and SPM as compared with the main lake. The most probable reasons for the different IOP of the Crescent Lake are listed as follows:

1) It is partially closed with less interaction with the main lake Naivasha and the river inlets.
2) Deeper depth creating less resuspension of sediment and turbidity
3) Its calmer than the main lake because the crescent island blocked the southeastern wind
4) The algal blooming time for the main lake and Crescent lake might be different

5.5.2 The inlets for Gilgil and Malewa Rivers,

The inlets for Gilgil and Malewa are the major source of sediment load into the lake. The sediment types consists of sandy mud and brown clay (Tarras-Wahlberg et al., 2002) . During wavy condition of the lake the sediment resuspension increase shallow parts of this area . Inaddtion the Malewa river contribute the high total phosphorous (1.4 g/m^2 per year) load into the lake (Kitaka et al., 2002) thus facilitating eutrophication and plant growth around in the northern part of the lake (Ngari et al., 2009). As seen on figure (5-13), high backscatter coefficient and Chl_a absorption value are indicated around the northern part of the lake. This extends further east during windy conditions (Tarras-Wahlberg et al., 2002).

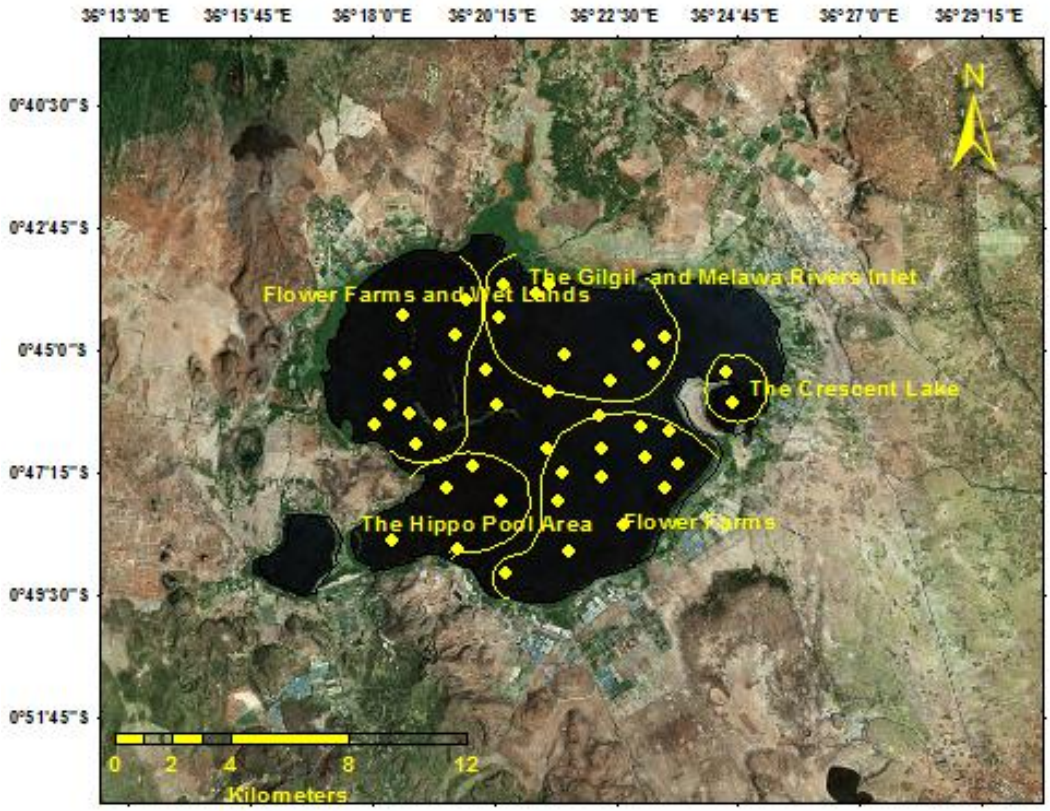

Figure 5-4: Spatial distribution of sampling points

5.5.3 Northwest part of the Lake Naivasha

The Northwest part of the lake is characterized by the floating plant, wetland area and flower farms. Most of the floating plants are transported in this area because of the southeast wind (major wind direction in the area) (Ngari et al., 2009). These plants are identified by their high Chl_a absorption (Figure 5-13, Figure 5-14). As a byproduct of the degradation or decay of the plants CDOM and NAP absorption is also higher in this area. Inaddtion the runoff from the flower farm located at the NNW could contribute to the enrichment of nutrient in the area.

NAP absorption significantly decrease during the second coverage of the lake. This is associated with the high backscattering of NAP from the resuspension of sediment during windy condition or due to mixing up of the water medium that settles the decayed organic matter.

5.5.4 Hippo pool and south-eastern flower farms

The Hippo pool is the deeper part of the lake that is inhabited mostly by hippopotamus. Between the hippo pool and the south eastern flower farm ,the public entry point called 'kamere' is located where several washing and animal herding takes place (Ngari et al., 2009). These areas are typically characterized by high nutrient. As seen from the map (Figure 5-13, Figure 5-14) the CDOM and Chl_a value are higher in these areas.

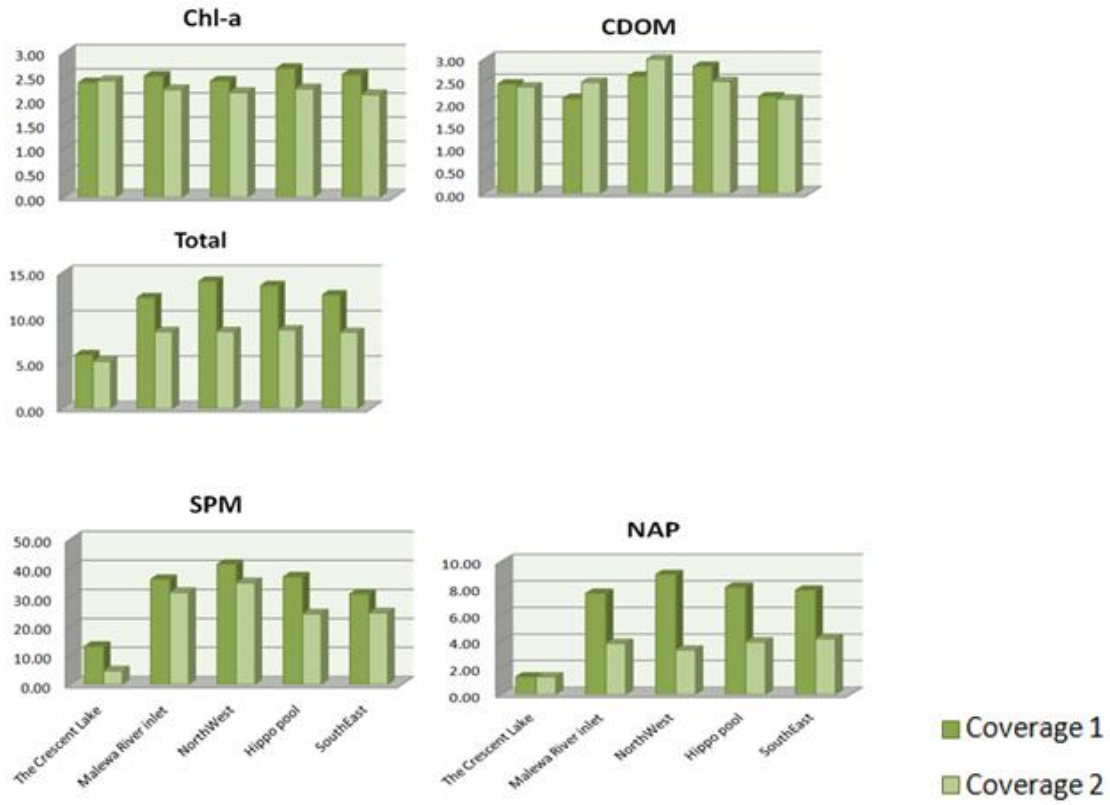

Figure 5-12 Spatial variation of IOPs within coverage one and two of the lake

5.2 Indicators of Eutrophication and Toxic algal blooms in the Lake Naivasha

The above observation and maps suggests that mixing by wind and wave action has a significant effect on increasing the eutrophication or the phytoplankton density (or suspended solids) at the surface. According to Kanoshina et al. (2003), During the algal bloom season once the continuous wave and the continuous turbulence mix the water body and the decrease in light penetration cause the phytoplankton to increase their buoyancy (2003). As soon as the wind stops, the phytoplankton (phycocyanin and Chl_a) floats rapidly towards the surface due to their over buoyancy (Figure 5-13). The formation of patches of algal colony in the lake is the result of low wind energy for re dispersing the algal into the water column. The high backscattering coefficient can be a good indicators of mixed up and resuspension of sediments from the shallow part of lake floor (especially located in the North near to the river inlets) (Everard et al., 2002). Inaddtion the high Chl_a and CDOM values along the northwest and southern part of lake also suggests the contribution of human activities such as intense farming and washing.

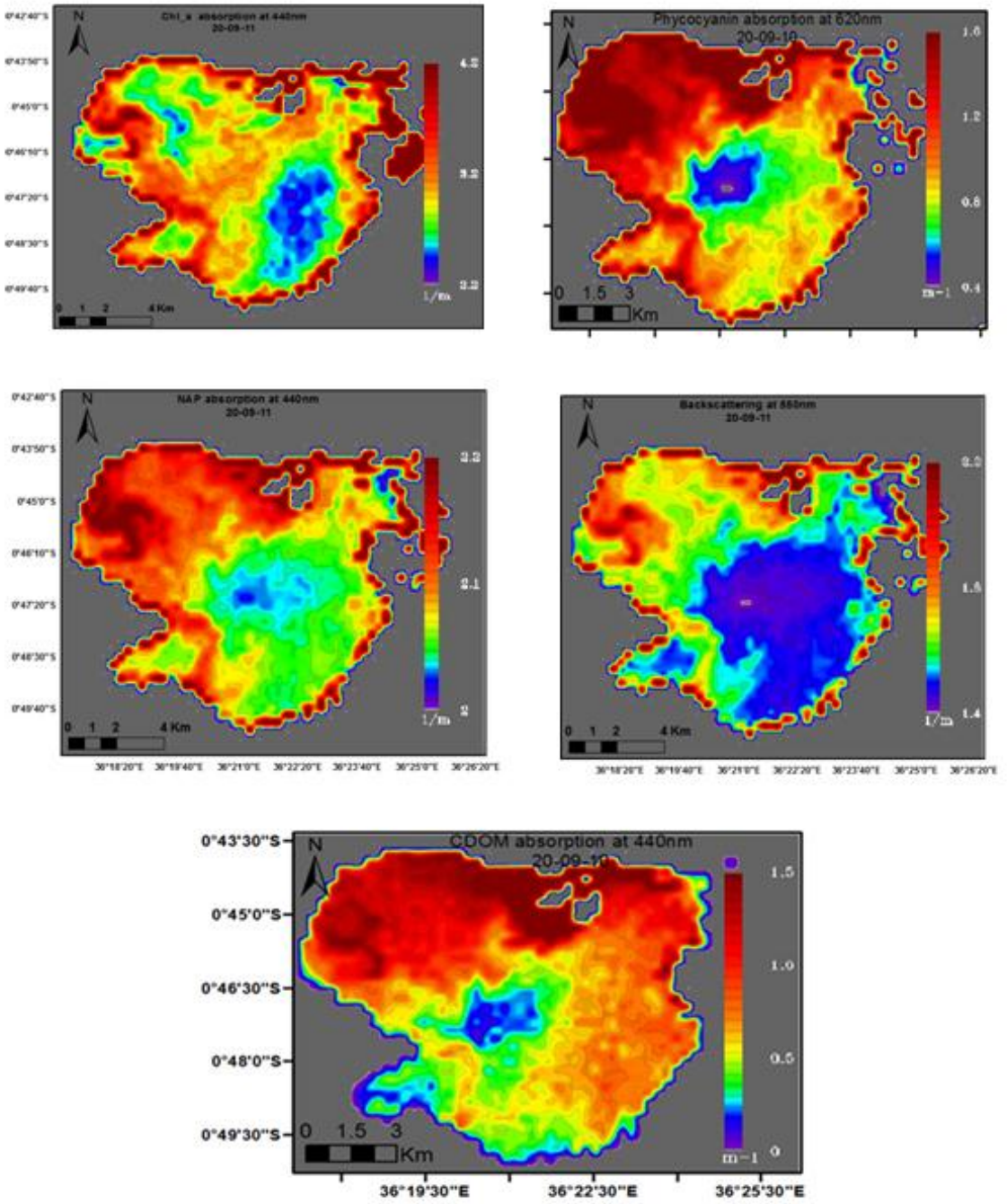

Figure 5-5 : Map that shows the distribution of derived IOPs using the MERIS image taken on 20/09/10.

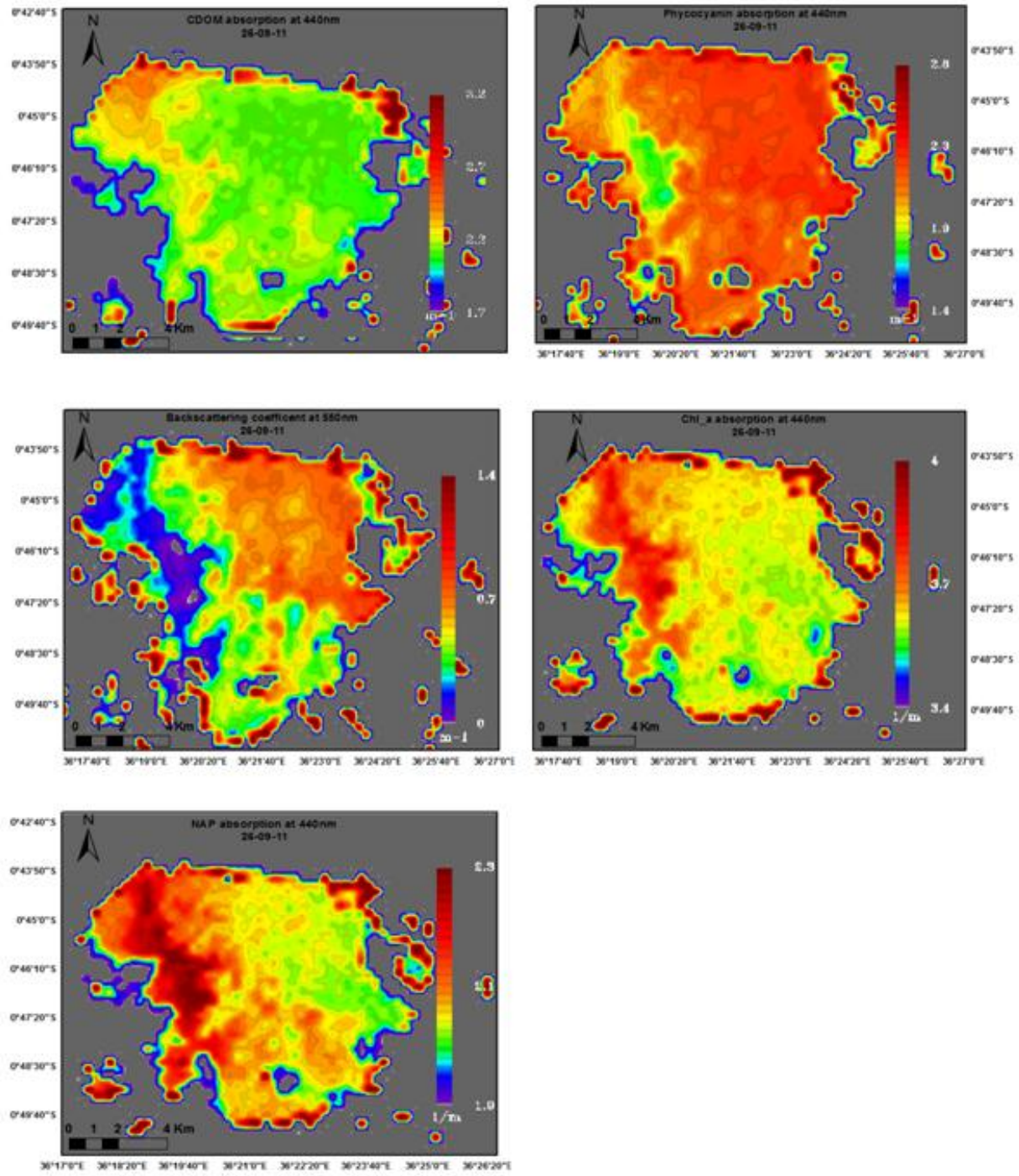

Figure 5-6: Map that shows the distribution of derived IOPs using the MERIS image taken on 26/09/10

6. CONCLUSION AND RECOMMENDATION

6.1 Conclusion

MERIS's relatively coarse spatial resolution was found to be good to derive inherent optical property of small lakes such as Naivasha. However, MERIS retrievals of NAP were less accurate in comparison to TRIOS. This could be due to the spectral resolution of MERIS and hence the fewer degree of freedom of the inversion model.The modified algorithm shows a strong linear correlation between the insitu measured and estimate of IOPs. The phycocyanin absorption co varies with the Chl_a absorption, thus indicating the accuracy of the model inversion for the retrieval of phycocyanin absorption. The uncertainty of the inversion model decreased to a certain level and then starts increasing with water turbidity.

The basic conclusions that can be made on the water quality status of Lake Naivasha are as follows:

- The Fresh water Lake Naivasha is turned to eutrophic and optically turbid. It shows a high Chl_a and CDOM absorption >3 m^{-1} along the northwest and southern parts of the lake. The flower farms located in the southwest and the hippo pool areas are the major contributors of high nutrient load.
- NAP absorption plays a major role in total absorption~52%. The maximum NAP has been observed at the inlet of the river Malewa and Gilgil inlets. The typical sediment load found in this sites are composed of brown clay and sand mud .indicated the reason for the high absorption and backscattering value for the NAP.
- The environmental condition especially wind direction play a major role in the spatial distribution of the IOPs in the lake. One of the main contributions could be the resuspension of settled sediment at the bottom and algal bloom formation.
- The Crescent Lake shows totally different IOP as compared with the main lake. It has higher Chl_a content than the main lake but very low SPM and CDOM value has been recorded in the lake.
- The Phycocyanin has also proven to be covering most part of the main lake at the time of study. The present condition of the lake (shallow, nutrient enrich and warm temperature) the possibility of toxic algal blooms such as cyanobacteria is high.
- Hyper spectral resolution is needed to be able to de-convolve the contribution of NAP to the total absorption of water constituents

6.2 Recommendation

The Lake Naivasha is gradually turning to eutrophic lake despite the fact that it's one of the most important lakes as both economical and recreational area in Kenya. The uncertainty of modified model decreases with higher absorption of Chl_a and phycocyanin. This outcome is very interesting to study the spatial and temporal variability of algal blooms in the lake Naivasha using MERIS. One limitation could be higher probability of cloud coverage of the Lake makes it difficult to time series analysis.

The modified GSM algorithms can be optimized to local purpose by cooperating the specific inherent optical property measurement of samples this will reduce the number of unknown in the mode.

LIST OF REFERENCES

Babin, M., Morel, A., Fournier-Sicre, V., Fell, F., & Stramski, D. (2003). Light scattering properties of marine particles in coastal and open ocean waters as related to the particle mass concentration. *Limnology and Oceanography, 48*(2), 843-859.

Ballot, A., Kotut, K., Novelo, E., & Krienitz, L. (2009). Changes of phytoplankton communities in Lakes Naivasha and Oloidien, examples of degradation and salinization of lakes in the Kenyan Rift Valley. *Hydrobiologia, 632*(1), 359-363.

Becht, R., & Harper, D. M. (2002). Towards an understanding of human impact upon the hydrology of Lake Naivasha, Kenya. *Hydrobiologia, 488*(1), 1-11.

Binding, C. E., Jerome, J. H., Bukata, R. P., & Booty, W. G. (2008). Spectral absorption properties of dissolved and particulate matter in Lake Erie. *Remote Sensing of Environment, 112*(4), 1702-1711.

Bricaud, A., Morel, A., Babin, M., Allali, K., & Claustre, H. (1998). Variations of light absorption by suspended particles with chlorophyll a concentration in oceanic (case 1) waters: Analysis and implications for bio-optical models. *Journal of Geophysical Research-Oceans, 103*(C13), 31033-31044.

Bricaud, A., Morel, A., & Louis, P. (1981). Absorption by dissolved organic matter of the sea(yellow substance) in UV and visible domains. *Limnology and Oceanography, 26(1)*, 43-53.

Codd, G. A. (2000). Cyanobacterial toxins, the perception of water quality, and the prioritisation of eutrophication control. [doi: DOI: 10.1016/S0925-8574(00)00089-6]. *Ecological Engineering, 16*(1), 51-60.

Dekker, A. G., Malthus, T. J., & Seyhan, E. (1991). Quantitative modeling of inland water quality for high-resolution MSS systems. *Geoscience and Remote Sensing, IEEE Transactions on, 29*(1), 89-95.

Deschamps, P. Y., Herman, M., & Tanre, D. (1983). Definitions of atmospheric radiance and transmittances in remote sensing. [doi: DOI: 10.1016/0034-4257(83)90029-9]. *Remote Sensing of Environment, 13*(1), 89-92.

Doxaran, Froidefond, J. M., Lavender, S., & Castaing, P. (2002). Spectral signature of highly turbid waters - Application with SPOT data to quantify suspended particulate matter concentrations. *Remote Sensing of Environment, 81*(1), 149-161.

Doxaran, D., Babin, M., & Leymarie, E. (2007). Near-infrared light scattering by particles in coastal waters. *Optics Express, 15*(20), 12834-12849.

Doxaran, D., Ruddick, K., McKee, D., Gentili, B., Tailliez, D., Chami, M., & Babin, M. (2009). Spectral variations of light scattering by marine particles in coastal waters, from visible to near infrared. *Limnology and Oceanography, 54*(4), 1257-1271.

Eisma, D., & Kalf, J. (1987). Distribution, organic content and particle size of suspended matter in the north sea. [doi: DOI: 10.1016/0077-7579(87)90002-0]. *Netherlands Journal of Sea Research, 21*(4), 265-285.

Everard, M., Vale, J. A., Harper, D. M., & Tarras-Wahlberg, H. (2002). The physical attributes of the Lake Naivasha catchment rivers. *Hydrobiologia, 488*(1-3), 13-25.

Fitch, D. T., & Moore, J. K. (2007). Wind speed influence on phytoplankton bloom dynamics in the Southern Ocean Marginal Ice Zone. *J. Geophys. Res., 112*(C8), C08006.

G. Dall'Olmo, & A.A Gitelson. (2006). Absorption Properties of Dissolved and Particulate Matter in Turbid Productive Inland Lakes. *Ocean Optics XVIII*, 1-15.

Gallegos, C. L., & Neale, P. J. (2002). Partitioning Spectral Absorption in Case 2 Waters: Discrimination of Dissolved and Particulate Components. *Appl. Opt., 41*(21), 4220-4233.

Garver, S. A., & Siegel, D. A. (1997). Inherent optical property inversion of ocean color spectra and its biogeochemical interpretation 1. Time series from the Sargasso Sea. *J. Geophys. Res., 102*(C8), 18607-18625.

Gordon, H. R., Brown, O. B., Evans, R. H., Brown, J. W., Smith, R. C., Baker, K. S., & Clark, D. K. (1988). A semianalytic radiance model of ocean color. *J. Geophys. Res, 93*(D9), 10909–10924.

Gordon, H. R., Brown, O. B., & Jacobs, M. M. (1975). Computed Relationships Between the Inherent and Apparent Optical Properties of a Flat Homogeneous Ocean. *Appl. Opt., 14*(2), 417-427.

Gordon , H. R., Otic, B. B., Robert, H. E., James , W. B., Raymond, C. S., Karen , S. B., & Dennis, K. C. (1988). A semianalytic radiance model of ocean colour. *Journal of geophysical research, 93*, 909-924.

Guanter, L., Ruiz-Verdú, A., Odermatt, D., Giardino, C., Simis, S., Estellés, V., Heege, T., Domínguez-Gómez, J. A., & Moreno, J. (2010). Atmospheric correction of ENVISAT/MERIS data over

inland waters: Validation for European lakes. [doi: DOI: 10.1016/j.rse.2009.10.004]. *Remote Sensing of Environment, 114*(3), 467-480.
Harped, D. M., Adams, C., & Mavuti, K. (1995). The aquatic plant communities of the Lake Naivasha wetland, Kenya: pattern, dynamics and conservation. *Wetlands Ecology and Management, 3*(2), 111-123.
Harper, D. M., Boar, R., Everard, M., & Hickley, P. (2003). *Lake Naivasha, Kenya*.
Hommersom, A., Peters, S., Wernand, M. R., & de Boer, J. (2009). Spatial and temporal variability in bio-optical properties of the Wadden Sea. *Estuarine Coastal and Shelf Science, 83*(3), 360-370.
Kanoshina, I., Lips, U., & Leppänen, J.-M. (2003). The influence of weather conditions (temperature and wind) on cyanobacterial bloom development in the Gulf of Finland (Baltic Sea). [doi: DOI: 10.1016/S1568-9883(02)00085-9]. *Harmful Algae, 2*(1), 29-41.
Kirk, J. (1976). Yellow substance (gelbstoff) and its contribution to the attenuation of photosynthetically active radiation in some inland and coastal south-eastern Australian waters. *Marine and Freshwater Research, 27*, 61-71.
Kitaka, N., Harper, D. M., & Mavuti, K. M. (2002). Phosphorus inputs to Lake Naivasha, Kenya, from its catchment and the trophic state of the lake. *Hydrobiologia, 488*(1), 73-80.
Lee, Z., Carder, K. L., & Arnone, R. A. (2002). Deriving Inherent Optical Properties from Water Color: a Multiband Quasi-Analytical Algorithm for Optically Deep Waters. *Appl. Opt., 41*(27), 5755-5772.
Lee, Z., Carder, K. L., Mobley, C. D., Steward, R. G., & Patch, J. S. (1998). Hyperspectral Remote Sensing for Shallow Waters. I. A Semianalytical Model. *Appl. Opt., 37*(27), 6329-6338.
Lee, Z., Carder, K. L., Mobley, C. D., Steward, R. G., & Patch, J. S. (1999). Hyperspectral Remote Sensing for Shallow Waters. 2. Deriving Bottom Depths and Water Properties by Optimization. *Appl. Opt., 38*(18), 3831-3843.
M.Bates, D., & G.Watts, D. (1988). *Nonlinear Regresstion Anaylsis and Its applications*. NY: John Wiley and Sons.
Magnuson, A., Harding, J. L. W., Mallonee, M. E., & Adolf, J. E. (2004). Bio-optical model for Chesapeake Bay and the Middle Atlantic Bight. [doi: DOI: 10.1016/j.ecss.2004.06.020]. *Estuarine, Coastal and Shelf Science, 61*(3), 403-424.
Maritorena, S., & Siegel, D. A. (2005). Consistent merging of satellite ocean color data sets using a bio-optical model. [doi: DOI: 10.1016/j.rse.2004.08.014]. *Remote Sensing of Environment, 94*(4), 429-440.
Maritorena, S., Siegel, D. A., & Peterson, A. R. (2002). Optimization of a semianalytical ocean color model for global-scale applications. *Appl. Opt., 41*(15), 2705-2714.
Matthews, M. W., Bernard, S., & Winter, K. (2010). Remote sensing of cyanobacteria-dominant algal blooms and water quality parameters in Zeekoevlei, a small hypertrophic lake, using MERIS. [doi: DOI: 10.1016/j.rse.2010.04.013]. *Remote Sensing of Environment, 114*(9), 2070-2087.
Melin, F. (2010). Global Distribution of the Random Uncertainty Associated With Satellite derived Chl-a. *Geoscience and Remote Sensing Letters, IEEE, 7*(1), 220-224.
Moran, M. S., Jackson, R. D., Slater, P. N., & Teillet, P. M. (1992). Evaluation of simplified procedures for retrieval of land surface reflectance factors from satellite sensor output. [doi: DOI: 10.1016/0034-4257(92)90076-V]. *Remote Sensing of Environment, 41*(2-3), 169-184.
Morel, A. (1974). Optical properties of pure water and pure sea water.
Morel, A., & Bélanger, S. (2006). Improved detection of turbid waters from ocean color sensors information. *Remote Sensing of Environment, 102*(3-4), 237-249.
Morel, A., & Louis, P. (1977). Analysis of variation in ocean colour. *Limnology and Oceanography, 22*, 709-722.
Morel, A., & Maritorena, S. (2001). Bio-optical properties of oceanic waters: A reappraisal. *J. Geophys. Res., 106*(C4), 7163-7180.
Moreno-Ostos, E., Cruz-Pizarro, L., Basanta, A., & George, D. (2009). The influence of wind-induced mixing on the vertical distribution of buoyant and sinking phytoplankton species. *Aquatic Ecology, 43*(2), 271-284.
Mueller, J. L., G.S. Fargion, & C.R. McClain, E. (2003). Ocean Optics Protocols for Satellite Ocean Color Sensor Validation, Revision 4 ,Volume IV: Inherent Optical Properties:Instruments, Characterizations, Field Measurements and Data Analysis Protocols. *NASA Tech.* .
Neckel, H., & Labs, D. (1981). Improved data of solar spectral irradiance from 0.33 to 1.25μ. *Solar Physics, 74*(1), 231-249.

Ngari, A. N., Kinyamario, J. I., Ntiba, M. J., & Mavuti, K. M. (2009). Factors affecting abundance and distribution of submerged and floating macrophytes in Lake Naivasha, Kenya. *African Journal of Ecology, 47*(1), 32-39.

Njenga, J. W., Ramanathan, A. L., & Subramanian, V. (2009). Partitioning of heavy metals in the sediments of Lake Naivasha, Kenya. *Chemical Speciation and Bioavailability, 21*(1), 41-48.

Pope, R. M., & Fry, E. S. (1997). Absorption spectrum (380-700 nm) of pure water. II. Integrating cavity measurements. *Appl. Opt., 36*(33), 8710-8723.

Rupasingha, R. A. P. (2002). *Use of GIS and RS for assessing lake sedimentation processes : case study for Naivasha Lake, Kenya*. ITC, Enschede.

Salama, M. S., Dekker, A., Su, Z., Mannaerts, C. M., & Verhoef, W. (2009). Deriving inherent optical properties and associated inversion-uncertainties in the Dutch Lakes. *Hydrology and Earth System Sciences, 13*(7), 1113-1121.

Salama, M. S., & Stein, A. (2009). Error decomposition and estimation of inherent optical properties. *Appl. Opt., 48*(26), 4947-4962.

Siegel, D. A., Wang, M., Maritorena, S., & Robinson, W. (2000). Atmospheric Correction of Satellite Ocean Color Imagery: The Black Pixel Assumption. *Appl. Opt., 39*(21), 3582-3591.

Simis, S. G. H., Tijdens, M., Hoogveld, H. L., & Gons, H. J. (2005). Optical changes associated with cyanobacterial bloom termination by viral lysis. *Journal of Plankton Research, 27*(9), 937-949.

Smyth, G. K. (2006). *NonLinear Regression*: John Wiley & Sons, Ltd.

Stedmon, C. A., Markager, S., & Kaas, H. (2000). Optical Properties and Signatures of Chromophoric Dissolved Organic Matter (CDOM) in Danish Coastal Waters. [doi: DOI: 10.1006/ecss.2000.0645]. *Estuarine, Coastal and Shelf Science, 51*(2), 267-278.

Sun, D. Y., Li, Y. M., Wang, Q., Le, C. F., Huang, C. C., & Wang, L. Z. (2009). Parameterization of water component absorption in an inland eutrophic lake and its seasonal variability: a case study in Lake Taihu. [Article]. *International Journal of Remote Sensing, 30*(13), 3549-3571.

Tarras-Wahlberg, H., Everard, M., & Harper, D. M. (2002). Geochemical and physical characteristics of river and lake sediments at Naivasha, Kenya. *Hydrobiologia, 488*(1-3), 27-41.

Wrigley, R. C., & Horne, A. J. (1974). Remote sensing and lake eutrophication. [10.1038/250213a0]. *Nature, 250*(5463), 213-214.

Zhang, Y. L., Zhang, B., Wang, X., Li, J. S., Feng, S., Zhao, Q. H., Liu, M. L., & Qin, B. Q. (2007). A study of absorption characteristics of chromophoric dissolved organic matter and particles in Lake Taihu, China. *Hydrobiologia, 592*, 105-120.

APPENDICES

1 The Rhopath and Transmittance Value

MERIS wavelength	20-Sep-10			23-Sep-10			26-Sep-10		
	RMSE	rho path	Tv	RMSE	rho path	Tv	RMSE	rho path	Tv
412.69	0.0058	0.1181	1	0.0028	0.1239	0.4568	0.0093	0.1291	0.4231
442.56	0.0059	0.0894	1	0.0030	0.0957	0.5435	0.0093	0.1033	0.5731
489.88	0.0061	0.0573	1	0.0030	0.0684	0.6086	0.0091	0.0776	0.6748
509.82	0.0064	0.0455	1	0.0035	0.0581	0.6665	0.0090	0.0722	0.6228
559.69	0.0080	0.0201	1	0.0049	0.0405	0.7446	0.0094	0.0647	0.5976
619.60	0.0093	0.0132	1	0.0046	0.0275	0.7939	0.0089	0.0479	0.7005
664.57	0.0096	0.0121	1	0.0044	0.0224	0.8626	0.0091	0.0387	0.8652
680.82	0.0097	0.0118	1	0.0043	0.0209	0.8628	0.0089	0.0320	1
708.33	0.0121	0.0058	1	0.0060	0.0164	0.9421	0.0094	0.0474	0.7155
753.37	0.0200	0.0169	1	0.0083	0.0181	1	0.0091	0.0345	1
761.51	0.0146	-0.0175	1	0.0062	-0.0105	1	0.0079	-0.0053	1
778.41	0.0207	0.0160	1	0.0087	0.0172	1	0.0089	0.0336	1
864.88	0.0229	0.0167	1	0.0083	0.0152	1	0.0087	0.0327	1
884.94	0.0234	0.0163	1	0.0084	0.0144	1	0.0087	0.0314	1
900.00	0.0186	0.0066	1	0.0065	0.0088	1	0.0069	0.0195	1

2 The Specification Of MERIS Sensor

Geometric Image Quality	
Field of view	68.5^{0}centred about nadir
Swath width	1150 km
Localization of accuracy	<2 km (without the use of land marks)
Spatial resolution	RR: 1040m X 300m (nadir)
	FR:260m X 300m (nadir)
Band to band registration	<0.1 FR pixel
Spectrometric Image Quality	
Spectral range	390 nm-1040 nm
Spectral sampling interval	1.25nm
Spectral resolution	1.8nm
Band transmission capability	15 bands programmable in position and width
Band width	Programmable from 1.25nm up to 30nm
Band centre knowledge	<0.6nm
Radiometric Image Quality	
Radiometric accuracy	<2% in reflectance(i.e. relative the sun irradiance)
Dynamic range	Up to bright clouds (100% reflectance)
Signal to noise ratio	1650(@412.5nm) for typical ocean signal
Polarisation sensitivity	<0.3% over the full spectral range
Orbital signal stability	<0.05%

3. Least-Square Minimization

The approach to retrieve the IOP from recorded reflectance is to maximize the probability of the IOP that give the observed water leaving reflectance. The water leaving reflectance modelled as a set of data; a point for each band. The measurement error of the water leaving reflectance at each band can be assumed normally distributed around the model output (the mean). The probability distribution function of the data set is proportional to the product of each probability at each band:

$$P \approx \prod_{i=1}^{N}\left\{exp\left(-\frac{1}{2}\left[\frac{Rrs_{w,m}^{(\lambda_i)}-Rrs_{w,d}^{(\lambda_i)}(IOP)}{\sigma_i}\right]^2\right)\Delta Rrs_w\right\} \quad \text{App 1}$$

Where $Rrs_{w,m}^{(\lambda_i)}$ is recorded water leaving reflectance and $Rrs_{w,d}^{(\lambda_i)}(IOP)$ is the derived reflectance as a function of the IOP's vector IOP; σ_i is the standared deviation of the measurement at the band I. Maximizing Eqn(4.11) is the same as maximizing its logarithm, or minimizing the negative of its logarithm:

$$\frac{1}{2}\sum_{i=1}^{N}\left[\frac{Rrs_{w,m}^{(\lambda_i)}-Rrs_{w,d}^{(\lambda_i)}(IOP)}{\sigma_i}\right]^2 - Nlog\Delta Rrs_w \quad \text{App 2}$$

The number of bands N and the derivative ΔRrs_w can be assumed constant, minimizing Eqn (4.12) is equivalent to minimizing the following:

$$\chi^2 = \sum_{i=1}^{N}\left[\frac{Rrs_{w,m}^{(\lambda_i)}-Rrs_{w,d}^{(\lambda_i)}(IOP)}{\sigma_i}\right]^2 \quad \text{App 3}$$

The quantity in (4.13) is called the chi-square (χ^2). This corresponds to the sum of N squares of normally distributed quantities, each normalized to a unit variance. If the variance can be assumed constant for all channels then the minimization in Eq.4.13 is simplified to:

$$\emptyset = \sum_{i=1}^{N}\left[Rrs_{w,m}^{(\lambda_i)} - Rrs_{w,d}^{(\lambda_i)}(IOP)\right]^2 \quad \text{App 4}$$

From the above discussion, we can conclude that least-square minimization is a special case of chi-square minimization (maximum likelihood estimation) of the fitted parameters. This is true taking into account our first assumption of normally distributed errors with a constant standard deviation.

Once the Eqn (4.14) start iterating (i) with the initial values, in each iteration (i) the values of the IOP are adjusted to decrease the cost of function ($\emptyset_{i+1} < \emptyset_i$).This is preceded until the cost of function has converged to minimum. The initial values are adapted from Lee et al. (1999) and values for Scdom and S_{nap}; 0.021 and 0.001 respectively as adapted from IOCCG report (Mueller et al., 2003).

$$a_{ph}(440) = 0.072\left(\frac{R_{rs}^{(440)}}{R_{rs}^{(550)}}\right)^{-1.62} \quad \text{App 5}$$

$$a_{nap}(440) = a_{ph}(440) \quad \text{App 6}$$

$$a_{cdom}(440) = a_{ph}(440) \quad \text{App 7}$$

$$bb_{spm}(550) = 30a_w(640)R_{rs}(640) \quad \text{App 8}$$

$$\gamma = 3.44\left(1 - 3.17\exp(-2.01\,(R_{rs}^{(550)})\right) \quad \text{App 9}$$